Title: Myc and Tor drive growth and cell competition in the regeneration blastema of *Drosophila* wing imaginal discs

Running title: Myc and Tor in Regeneration

Felicity Ting-Yu Hsu[1] and Rachel Smith-Bolton[1]

[1] Cell and Developmental Biology, University of Illinois at Urbana-Champaign, Urbana, IL 61801, USA

*Author for correspondence (rsbolton@illinois.edu)

Keywords: Regeneration, Drosophila, Myc, Tor, Cell Competition

Summary statement

Drosophila wing disc regeneration is characterized by concentric growth zones controlled by the Myc transcription factor, the Tor signaling pathway, and Myc-induced cell competition.

Abstract

During the regeneration of injured or lost tissues, the regeneration blastema serves as a hub for robust growth. *Drosophila* imaginal discs are a genetically tractable and simple model system for the study of regeneration and organization of this regrowth. Key signals that contribute to regenerative growth in these discs, such as ROS, Wnt/Wg, JNK, p38, JAK/STAT, and the Hippo pathway, have been identified. However, a detailed exploration of the spatial organization of regrowth, the factors that directly drive this growth, and the consequences of activating drivers of regeneration has not been undertaken. Here, we find that regenerative growth in imaginal discs is controlled by the transcription factor Myc and by Tor signaling, which additively drive proliferation and translation in the regeneration blastema. The spatial organization of growth in the blastema is arranged into concentric growth zones defined by Myc expression, elevated Tor activity, and elevated translation. In addition, the increased Myc expression in the innermost zone induced Xrp1-independent cell competition-like death in the adjacent zones, revealing a delicate balance between driving growth and inducing death in the regenerating tissue.

Introduction

Regeneration is a phenomenon through which some animals restore tissues or organs after damage. This regrowth often occurs through proliferation of a group of undifferentiated and robustly growing cells at the damage site, called a blastema (reviewed in Londono et al., 2018). To study tissue regeneration, we use *Drosophila* wing imaginal discs as a model. The ability of these appendage primordia to regenerate during the larval stage was discovered when the imaginal discs were cut and incubated in the abdomens of female flies (Hadorn and Buck, 1962). Two decades later, blastema-like cells were shown to be robustly proliferating at the wound site in leg and wing imaginal discs (Abbott et al., 1981; O'Brochta and Bryant, 1987). Subsequent searches for signaling pathways important for regenerative growth identified Jun N-terminal Kinase (JNK) signaling as crucial for disc regeneration after fragmentation (Bosch et al., 2005), and lineage tracing demonstrated that cells experiencing JNK signaling were the origin of the regeneration blastema (Bosch et al., 2008). More recently, genetic ablation systems have replaced fragmentation in regeneration studies, where localized massive cell death is generated through overexpression of pro-apoptotic genes (Fox et al., 2020). In these ablation systems, blastema cells were also found around the wound sites during regeneration (Smith-Bolton et al., 2009). To better define the blastema, two research groups (Floc'hlay et al., 2023; Worley et al., 2022) used single-cell RNA-sequencing (scRNA-seq) to characterize blastema cells by gene expression. This approach identified two clusters of cells with expression of signaling molecules such as Wg and Upd3 and transcription factors such as Ets21C that define the blastema (Floc'hlay et al., 2023; Worley et al., 2022). However, gene expression alone may not capture all changes in cell behavior and may not identify all cells contributing to the regenerating tissue.

The ability of imaginal discs to form a blastema is reduced during the late third instar due to an increase in the hormone ecdysone, which silences damage-responsive signals (Halme et al., 2010; Harris et al., 2016; Jaszczak and Halme, 2016). During normal development, low ecdysone levels maintain larval development and growth of the imaginal discs, while a burst of high ecdysone production triggers developmental transitions such as molting or pupariation (Thummel, 2001). Damage during the early-

and mid-third larval instar induces secretion of the relaxin-like peptide *Drosophila* insulin-like peptide 8 (ILP8), which reduces systemic ecdysone and delays the surge to prolong larval development. This reduced ecdysone also reduces imaginal disc growth outside of the damaged area (Colombani et al., 2012; Garelli et al., 2012; Halme et al., 2010; Jaszczak and Halme, 2016; Jaszczak et al., 2015; Jaszczak et al., 2016; Karanja et al., 2022; Katsuyama et al., 2015). Therefore, the regeneration blastema must override the global reduction of growth due to low ecdysone levels.

In this paper, we demonstrate that two factors drive blastema growth additively – the transcription factor Myc and the Target of Rapamycin (Tor) signaling pathway. Both Myc transcription and Tor signaling were upregulated during regeneration. Reducing their expression or kinase activity reduced proliferation and translation in the blastema. Interestingly, the area with activated Tor signaling extended beyond the area with high Myc expression, establishing concentric zones of blastema growth.

Myc expression level differences between adjacent cell populations lead to cell competition or super-competition during normal development (De La Cova et al., 2004; De La Cova et al., 2014; Meyer et al., 2014; Morata, 2021). Cell competition occurs when neighboring cells have different fitness levels, and “loser cells” are eliminated by cell death, while “winner cells” replace the loser cells, and a range of mechanisms have been proposed to carry out the fitness comparison (Reviewed in Morata, 2021). Death of the loser cells can involve autophagy (Nagata et al., 2019) and expression of the transcription factor Xrp1 (Baillon et al., 2018; Blanco et al., 2020; Kiparaki et al., 2022; Lee et al., 2018; Ochi et al., 2021).

Interestingly, proteotoxic stress as assessed by increased levels of phosphorylated eIF2α has been reported in loser cells during cell competition induced by mutations in ribosome genes (Baumgartner et al., 2021), and phosphorylated eIF2α is sufficient to induce loser cell fate (Kiparaki et al., 2022). However, increased phosphorylation of eIF2α also occurs in winner cells during super-competition induced by Myc overexpression, although these

cells are protected from this proteotoxic stress and do not undergo apoptosis (Paul et al., 2024).

Notably, these mechanisms that govern cell competition in wing imaginal discs have predominantly been studied using induced clones of genetically distinct cell populations (Reviewed in Khandekar and Ellis, 2024). While the regeneration blastema has high expression of Myc, it was unclear whether the Myc expression differences that arose during regeneration would lead to competitive behaviors similar to those induced by clones of cells in an undamaged disc and whether the mechanism would align with any of the established models of cell competition.

Here, we show that cell death is increased in the cells adjacent to the high Myc-expressing cells in the blastema. Furthermore, this cell death was suppressed when Myc expression was reduced. The cells adjacent to the high-Myc cells showed an increase in autophagy and eIF2α phosphorylation, similar to loser cells in cell competition. However, we did not find elevated Xrp1 expression, and heterozygosity for Xrp1 did not eliminate Myc-induced cell death in regenerating wing discs. Therefore, the heterogeneity and complex signaling in the regeneration blastema likely leads to a type of cell competition that is not identical to the competition induced when two sets of cells differ by only one factor.

Thus, wing disc regeneration involves not only robust regrowth but also increased cell death, suggesting that there is a dynamic balance between growth and death, providing new insights into the microenvironment of regenerating tissue.

Results

Myc and Tor drive blastema growth

To study regeneration in the *Drosophila* wing imaginal disc, we used a genetic ablation system in which tissue damage can be induced with spatial and temporal precision (Smith-Bolton et al., 2009). This ablation system uses the UAS/Gal4 transcriptional system, where a Gal4 in the *rotund* (*rn*) locus directs the expression of the pro-apoptotic gene *reaper* (*rpr*) in the wing imaginal disc pouch (Fig. 1A). In addition, the Gal4 activity

is constrained by Gal80^{ts} at 18°C but not at 30°C. We raised the larvae in an 18°C incubator for seven days after egg-laying, when the larvae reach the early third instar stage, then transferred the larvae to a 30°C water bath for 24 hours to activate apoptosis. After the 24-hour temperature shift, the larvae were returned to 18°C. This time point was considered recovery time 0 (R0) (Fig. 1A).

To characterize growth in a regenerating wing disc, we examined proliferation in undamaged and regenerating discs 24 hours after the end of tissue damage, or recovery time 24 (R24). We used EdU incorporation to mark cells in S-phase and anti-phospho-histone H3 (PH3) immunostaining to mark cells in mitosis. We compared the undamaged wing pouch, whose outer edge is marked by the inner ring of Wg expression (Fig. S1A,A')(Swarup and Verheyen, 2012), and the regeneration blastema, which is marked by Wg expression throughout (Fig. S1B,B') (Smith-Bolton et al., 2009; Worley et al., 2022). In undamaged wing discs, cells in S-phase were distributed evenly throughout the wing disc (Fig. 1B). However, after tissue damage, the blastema had increased EdU incorporation (Fig. 1C,D), suggesting more cells were in S phase. Similarly, mitotic cells appeared uniform throughout an undamaged wing disc (Fig. 1E), but the regeneration blastema had an increased number of mitotic cells (Fig. 1E,F,G).

Next, we asked if regeneration also involves increased growth driven by protein translation. To examine protein translation, we used the O-propargyl-puromycin (OPP) assay, which marks newly synthesized protein by incorporating a puromycin analog detected by click chemistry. In undamaged discs, translation seemed evenly distributed throughout (Fig. 1H). However, after tissue damage, the blastema had markedly increased translation (Fig. 1I,J).

Given that proliferation and translation were elevated in the regeneration blastema, we asked what drives this robust growth. To answer this question, we examined Ecdysone Receptor (EcR) activity, glycolysis, Myc expression, and Tor signaling. We first asked whether blastema cells escape reduced growth caused by reduced ecdysone by upregulating activity of the EcR (Fig. S1). Indeed, our transcriptional profile of the

regeneration blastema showed slight upregulation of *EcR*, a log2 increase of 1.16 (p=0.00005)(Khan et al., 2017). In addition, EcR activity is increased during later regeneration (R32) and is important for regeneration (Terry et al., 2024). To assess EcR activity at R24 we used the *7xEcRE-GFP* reporter, which has seven EcR response elements (EcREs) upstream of GFP (Hackney et al., 2007; Terry et al., 2024). In undamaged wing discs, the EcRE-GFP reporter was active in the entire wing pouch (Fig. S1C), and was not elevated in the blastema at R24 (Fig. S1D), indicating that enhanced EcR activity does not drive growth at R24.

Recent work on zebra fish fin regeneration demonstrated that glycolysis is increased during early regeneration due to the upregulation of lactate dehydrogenase (Ldh) (Brandão et al., 2022). Therefore, we asked whether increased glycolysis and lactate dehydrogenase might be driving the growth in the regeneration blastema. We used a reporter line for *Lactate dehydrogenase* (*Ldh*) expression, *Ldh-GFP*^{Genomic} (Bawa et al., 2020; Rai et al., 2024), which did not show increased expression in the blastema (Fig. S1E,F). Thus, upregulated Ldh does not drive the robust growth in the regeneration blastema.

Myc is a transcription factor that regulates cell growth by promoting proliferation and translation (Bellosta and Gallant, 2010; Grewal et al., 2005; Johnston et al., 1999) and is important for regeneration in multiple animals, including Hydra, Axolotl, *Xenopus*, and zebrafish (as reviewed in Ascanelli et al., 2024). In *Drosophila* imaginal discs, Myc is highly expressed in the blastema, overexpression of Myc leads to better regeneration, and reduction of Myc causes poor regeneration (Abidi et al., 2023; Harris et al., 2020; Serras and Bellosta, 2024; Smith-Bolton et al., 2009). To determine whether Myc is upregulated through transcription, we used a *Myc-lacZ* reporter line. In undamaged discs, *Myc-lacZ* expression was observed throughout the pouch, with a slight reduction at the dorsal-ventral boundary (Fig. 1K). At R24, *Myc-lacZ* was upregulated in the regeneration blastema (Fig. 1L-M). We previously found that Myc expression was difficult to reduce during regeneration, either through RNAi knockdown or use of a heterozygous mutation (Abidi et al., 2023), suggesting that its expression is tightly regulated.

Tor regulates translation by phosphorylating ribosomal p70 S6 kinase I (S6K), which in turn phosphorylates ribosomal protein S6 (RpS6) (reviewed in Frappaolo and Giansanti, 2023). We examined Tor pathway activity through anti-phospho-RpS6 (p-S6) immunostaining (Romero-Pozuelo et al., 2017). In an undamaged wing disc, elevated p-S6 occurred in a patchy pattern (Fig. 1N), consistent with previous studies (Romero-Pozuelo et al., 2017). At R24, p-S6 was enhanced in the regenerating blastema (Fig. 1O-P), suggesting that the Tor pathway might also be an important driver of growth during wing disc regeneration.

Myc promotes regenerative growth in a damaged wing disc

To determine the extent to which Myc contributes to the growth of the blastema, we examined proliferation and protein synthesis in regenerating wing discs with reduced Myc expression. We have previously shown that animals hemizygous for the hypomorphic allele Myc^{P0} had reduced Myc levels in regenerating wing discs and regenerated poorly (Abidi et al., 2023)(Fig. S2A,B). By comparing EdU incorporation in the control and the Myc^{P0} regeneration blastemas (Fig. 2A-B), we found a reduction in EdU when Myc levels were reduced (Fig. 2C). Similarly, measurement of mitoses by anti-PH3 staining showed fewer mitotic cells in the Myc^{P0} blastema (Fig. 2D-F). We used the OPP assay to measure protein translation and found that Myc^{P0} regenerating discs had reduced translation (Fig. 2G-I). Thus, Myc promotes growth in the regeneration blastema by promoting translation as well as proliferation.

As Myc regulates growth and translation at least partially through ribosomal biogenesis (Grewal et al., 2005), we examined ribosomal biogenesis by measuring the size of the nucleoli using an anti-Fibrillarin antibody. We measured 10 nucleoli in a 200-pixel^2 area in the hinge and pouch or blastema of each disc. In undamaged discs, the pouch nucleoli and the hinge nucleoli were similar in size (Fig. 2J-L,V). In regenerating wing discs, the blastema cells had larger nucleoli than the hinge cells (Fig. 2M-O,V). Importantly, the nucleoli in the blastema cells were also larger than those in undamaged discs (Fig. 2K,N,V).

To determine whether the larger nucleoli in the blastema were due to increased Myc expression, we measured nucleoli in undamaged and damaged Myc^{P0} discs. In Myc^{P0} undamaged discs, the nucleoli were the same size in the wing pouch and in the hinge (Fig. 2P-R,V) and smaller than those in control undamaged discs (Fig. 2V). This result was expected because Myc expression was reduced throughout the disc. In Myc^{P0} regenerating discs, nucleoli in the Myc^{P0} blastema were still larger than the nucleoli in the Myc^{P0} hinge (Fig. 2S-U,V) but were smaller than those in the control blastema (Fig. 2N,T,V). Therefore, Myc contributes to the growth of the regeneration blastema but does not account for all of the increase in ribosomal production and nucleolus size.

Tor promotes growth in the regeneration blastema

To determine the extent to which Tor signaling contributes to regeneration, we reduced Tor activity using animals heterozygous for Tor^{2L1}, a hypomorphic allele that has impaired kinase activity due to a single amino acid change in the kinase domain (Oldham et al., 2000). To confirm that Tor activity was reduced in Tor^{2L1}/+ regenerating discs, we assessed anti-p-S6 immunostaining at R24 (Fig. 3A-B), using Wg as a blastema marker (Fig. S3A-B). As expected, p-S6 signal was reduced in the blastemas of Tor^{2L1}/+ discs (Figs. 3A-C, S3A-B). In addition, we examined the adult wings that developed from regenerated discs of Tor^{2L1}/+ flies as a proxy for how well regeneration occurred in the imaginal disc. The Tor^{2L1}/+ flies had smaller wings after disc regeneration, indicating that the imaginal discs had regenerated poorly (Fig. S3C).

We assessed proliferation in Tor^{2L1}/+ regenerating discs using EdU incorporation and anti-PH3 staining (Figs. 3D-I, S3D-E). EdU intensity was reduced when Tor activity was reduced (Fig. 3D-F). Similarly, PH3 counts per area showed that the number of mitotic cells was reduced when Tor activity was reduced (Figs. 3G-I, S3D-E).

We examined protein translation using the OPP assay, and we found reduced protein translation in the blastema when Tor signaling was reduced (Figs. 3J-L, S3F-G). Thus, we concluded that Tor signaling promotes regeneration blastema growth by regulating

both proliferation and translation. Interestingly, we noticed that the blastema area, marked by Wg expression, was smaller than the area with upregulated translation (Fig. 3J-K), suggesting that regenerative growth may be elevated outside of the zone marked by expression of blastema genes.

Next, we asked if Tor enhances growth in part by enhancing ribosomal biogenesis. However, the nucleoli in the blastemas of *Tor*^{2L1}/+ discs were not smaller than those in the controls (Fig. S3H-N). We wondered if the heterozygous *Tor*^{2L1} allele was not strong enough for us to detect a requirement for Tor in ribosomal biogenesis. Therefore, we fed the larvae rapamycin to reduce Tor signaling (Fig. 3M-S). In both control and rapamycin-fed animals, the blastema cells had larger nucleoli than cells in the hinge (Fig. 3M,P). Interestingly, the rapamycin-fed animals had smaller nucleoli in the blastema compared to those in larvae fed control food (Fig. 3N,Q,S). Thus, Tor signaling is important for ribosome biogenesis.

Crosstalk between Tor signaling and Myc in the regeneration blastema

Several studies have shown interactions between Myc and Tor in regulating growth in *Drosophila* (Kuo et al., 2015; Parisi et al., 2011; Teleman et al., 2008). Thus, we asked whether there is also a crosstalk between Myc and Tor in the regeneration blastema. First, we asked whether regenerating discs with reduced Myc have reduced Tor activity by immunostaining for p-S6 in *Myc*^{P0}/*Y* regenerating discs and found reduced p-S6 intensity (Fig. S3O-P'). Thus, Myc is important for increased Tor signaling in the regeneration blastema.

Next, we asked if reduced Tor activity would reduce Myc expression in the regeneration blastema. We used rapamycin feeding to inhibit Tor activity and the *Myc-lacZ* reporter line to examine Myc transcription. We saw reduced transcription of the Myc reporter in the animals fed with rapamycin, compared to the animals fed with control food (Fig. S3R-T), suggesting that Tor signaling regulates Myc expression. Together, these results establish the existence of crosstalk between Myc and Tor signaling in the regeneration blastema.

Mapping the domain of high Myc expression in the regeneration blastema

Two sets of scRNA-seq data from regenerating *Drosophila* wing imaginal discs identified cells belonging to the regeneration blastema: called blastema 1 and blastema 2 cells (Worley et al., 2022), or wound alpha cells (Floc'hlay et al., 2023). The ablation assays used in these two studies were slightly different; we used the pro-apoptotic gene *reaper* to induce cell death whereas these studies used the TNFα *eiger*. In addition, Floc'hlay et al. activated ablation for 40 hours instead of the 24 hours that we and Worley et al. used. Therefore, to confirm that the expression of the blastema markers in our ablation system is similar to those identified in these reports, we used Upd3, a JAK/STAT ligand, as a blastema 1 marker and Wg as a blastema 1 and 2 marker (Worley et al., 2022). To visualize *upd3* expression, we used the reporter line *upd3-lacZ* (Bunker et al., 2015). In regenerating wing discs, we confirmed two zones in the regeneration blastema, in which the Wg-expressing area was larger than the *upd3-lacZ*-expressing area (Fig. 4 A-B'), confirming the existence of blastema 1 and 2 cells in our discs. To understand where Myc is upregulated, we used Wg as a blastema marker and co-immunostained for Myc. While Wg did not co-localize with Myc in an undamaged disc (Fig. 4C), in R24 discs, high Myc expression coincided with high Wg expression as previously reported (Smith-Bolton et al., 2009)(Fig. 4D-D').

We also determined the extent to which the blastema as defined by Worley et al. coincided with Nubbin (Nub) expression, which is normally found in the wing pouch and overlaps with the inner ring of Wg at the boundary between the pouch and the hinge (Ng et al., 1995; Terriente et al., 2008). In an undamaged wing disc, the Nub-expressing area was slightly larger than the moderate Myc-expressing area (Fig. 4E). During regeneration, the Nub-expressing area was also larger than the high Myc-expressing area (Fig. 4F-F'). Therefore, the blastema as defined by Wg and Myc expression is smaller than the Nub-expressing area. To determine which cells in the regenerating disc were hinge cells and if there is any overlap between the hinge and the regeneration blastema, we used a Zfh2 antibody (Tran et al., 2010) (Fig. 4G-H') and the JAK/STAT signaling reporter *10XSTAT92E-GFP* (Bach et al., 2007) (Fig. 4I-J') as hinge markers. In both undamaged

(Fig. 4G,I) and damaged discs (Fig. 4H-H',J-J'), the hinge markers were expressed directly adjacent to, but not overlapping with, the zone with elevated Myc expression.

To ask whether Nub and Zfh2 expression overlapped in regenerating discs, we used the *nub-MiMIC-GFP* (*nub*^{MI05126}) line, in which a MiMIC transposable element inserted into the *nub* locus expresses GFP in cells that are also marked with anti-Nub immunostaining (Khan et al., 2017; Venken et al., 2011b). In undamaged wing discs, Nub-GFP expression overlapped with Zfh2-positive cells at the inner ring of Wg expression (Fig. 4K), consistent with previous studies (Terriente et al., 2008). In regenerating wing discs, we also found Nub-GFP expression overlapping with Zfh2 expression (Fig. 4L). Furthermore, Wg, Nub, and Zfh2 expression together showed that the blastema was smaller than the Nub-expressing area but directly adjacent to the cells expressing both Nub and the hinge markers (Fig. 4L,L"). Interestingly, hinge cells adjacent to the blastema are flexible in their identity and can become pouch cells during re-growth (Herrera et al., 2013; Ledruet al., 2022; Worley et al., 2018), which may be occurring in the Nub-expressing (Nub+) Zfh2+ zone. Thus, the high Myc-expressing zone colocalized with the blastema as defined by single-cell sequencing and did not overlap with hinge cells.

The regeneration blastema includes additional zones of elevated growth outside the canonical blastema

While immunostaining for p-S6, we marked the blastema by immunostaining for Wg and found that the region with elevated Tor activity was larger than the area with Wg expression (Fig. 3A). In addition, the region marked with the OPP translation assay was also larger than the Wg-expressing area (Fig. 3J'). Thus, we sought to better understand the spatial relationships among the blastema, Myc expression, Tor signaling, and enhanced translation. Given that anti-Myc and anti-p-S6 are both rabbit antibodies, and that Myc and Wg expression co-localized, we used the Wg antibody to mark the Myc-expressing blastema cells. By visualizing Wg, p-S6, and translation, we discovered additional concentric zones of the regeneration blastema. Wg, marking the canonical blastema, was expressed in the center, which we call Growth Zone A (Fig. 5A,B), and which also had elevated p-S6 and OPP signal (Fig. 5C,D). Growth Zone B, the area

outside of Zone A, had high p-S6 but not Wg (Fig. 5A,C-E). Growth Zone C was the area with high translation but not upregulated Wg, Myc, or p-S6 (Fig. 5A,F-G). To confirm the existence of these zones, we quantified the area of each (Fig. 5H,I) and examined the fluorescence intensity profile of a cross-section through the wing disc (Fig. S5A-G'). Both analyses indicated that there were three distinct zones within the regeneration blastema.

We wondered whether the OPP signal in Zone C that extended beyond Zone B was caused by Tor signaling non-autonomously inducing increased translation, or by spread of the OPP signal, or by an unknown additional factor that increases translation. To test the extent to which Tor activity can induce OPP signal non-autonomously, we activated Tor in the posterior half of an undamaged wing disc using *hhGal4, UAS-Tsc2RNAi* (*hh>Tsc2i*) and performed the OPP assay and p-S6 immunostaining (Fig. S5H-Q). The elevated OPP signal extended beyond the A/P boundary while the p-S6 immunostaining did not (Fig. S5H-Q). Therefore, Tor activity can induce elevated translation in the adjacent cells or the OPP assay signal spreads, perhaps due to newly synthesized secreted or extracellular proteins labeled with OPP.

To determine whether Growth Zone C coincided with the Nub-expressing area, we combined the OPP assay with Nub immunostaining (Fig. 5J-L). The Nub+ area was slightly larger than the area with elevated translation, indicating that Growth Zone C is smaller than the remaining inner hinge (Fig. 5J-L).

The concentric growth zones have different proliferation rates

We wondered whether these blastema zones were biologically relevant. Therefore, we asked if cell proliferation was different across these zones. Given that anti-PH3 and anti-p-S6 are both rabbit antibodies, we could not use p-S6 to mark Zone B. Therefore, we took an approximate approach by measuring the area of each zone and calculating the average radius. We used the radii to determine the distances between the edges of Growth Zones A, B, and C. Using these measurements, the average distance between the edges of Growth Zone A and B was 13 microns, and the average distance between the edges of Growth Zone B and C was 16 microns (Fig. 5A,I). We then immunostained

for Wg to establish the boundary of Growth Zone A, and measured concentric zones based on the shape of Wg immunostaining (Fig. 5M). We then assessed mitoses per area in each zone (Fig. 5N). Proliferation was highest in Growth Zone A, was slightly reduced in Growth Zone B, and was even lower in Growth Zone C. Proliferation in the cells 10 microns outside of Growth Zone C was even lower. Thus, these growth zones are biologically meaningful and contribute at different levels to the regrown wing pouch.

Myc expression induces cell death at the periphery of Growth Zone A

Given the difference in Myc levels between Growth Zone A and the rest of the disc, we wondered whether cell competition was occurring. We quantitated cell death using the terminal d-UTP nick-end labeling (TUNEL) assay. Since we used apoptosis to induce tissue damage, we needed to distinguish between ablation and cell competition. We used *UAS-eGFP* to mark apoptotic cells eliminated by our ablation system. At R0, GFP-expressing debris was found on both the basal and the apical sides of the columnar epithelium, or disc proper (Fig. 6A). However, at R24, the GFP-containing debris on the basal side of the epithelium was mostly gone (Fig. 6B), and most of the TUNEL-positive cells did not express GFP (Fig. 6B).

Cells undergoing apoptosis due to cell competition are extruded toward the basal side of the epithelium (Amoyel and Bach, 2014; Li and Baker, 2007). In addition, cell death driven by Myc-induced super competition occurs within an eight-cell zone adjacent to the winner cells (De La Cova et al., 2004). To set a baseline for quantification, we quantified TUNEL in a negative control, in which *dpp-Gal4* was used to drive *UAS-GFP* in a normally developing wing disc*,* and a positive control, in which *dpp-Gal4* was used to drive *UAS-Myc*. In the negative control, there was no Myc expression difference and no TUNEL-positive cells (Fig. 6C,C',G). In the positive control, cell death was observed in cells located inside the high-Myc stripe and in cells located within an eight-cell region adjacent to the high-Myc cells (Fig. 6D,D',G). These results concurred with previous studies (De La Cova et al., 2004) and gave us a baseline for measuring cell competition due to elevated Myc expression.

We then quantified TUNEL-positive cells in regenerating discs that were on the basal side of the epithelium within an eight-cell-wide band outside of the Myc-expressing cells (Fig. 6E,E'). We found cell death at the basal side of regenerating wing discs that was even higher than in the positive controls (Fig. 6E-E',G). To determine whether this apoptosis was due to elevated Myc expression, we quantified TUNEL-positive cells in *Myc^{P0}* regenerating discs (Fig. 6F,F',G). Surprisingly, the overall number of TUNEL-positive cells on the basal side of the epithelium was not reduced in *Myc^{P0}* regenerating discs (Fig. 6G). However, the number of TUNEL-positive cells inside of the Wg+ zone in *Myc^{P0}* discs was higher (Fig. 6H,I) and cell death at the periphery of the Wg+ zone was significantly reduced (Fig. 6H,J). This finding suggests that the cell death observed outside of the Wg+ and Myc+ zone is due to Myc expression level differences. Furthermore, the increased cell death within the Wg+ zone in *Myc^{P0}* regenerating discs suggested that Myc is important for survival of these blastema cells. The blastema is subject to complex signaling interactions due to the damage response, which may lead to this requirement for elevated Myc for cell survival.

Cell competition induced in regenerating wing discs is distinct from experimentally induced cell competition

Cell competition and super-competition studies usually involve genetic clones that differ by one or two factors relative to the surrounding cells, experimentally establishing a mismatch in cell fitness. However, in regenerating imaginal discs, there are overlapping and adjacent zones of elevated Wg, JAK/STAT, Yki, JNK, p38, and Tor signaling (Bergantiños et al., 2010; Grusche et al., 2011; Santabárbara-Ruiz et al., 2015; Smith-Bolton et al., 2009; Sun and Irvine, 2011) (Figs. 4C-D',I-J', 5B,E), which may render fitness comparisons during regeneration more complex than the binary comparisons made in cell competition studies. Therefore, to ask whether the cells outside the high Myc zone were behaving like "loser cells", we examined three different factors that are important for loser cell fate in cell competition and super-competition, including proteotoxic stress, autophagy, and expression of Xrp1.

The distinction between cell competition and super-competition is based on whether wild-type cells are winner cells or loser cells (Morata, 2021). However, it is unclear whether the cells outside of the high-Myc zone in regenerating discs can be described as wild-type cells because Myc levels are lower than in normal discs. In addition, Myc levels in the blastema are elevated relative to the rest of the disc and relative to undamaged discs but are not as high as when Myc is overexpressed. Given that loser cells during cell competition have increased eIF2α phosphorylation due to proteotoxic stress (Baumgartner et al., 2021; Kiparaki et al., 2022), and winner cells during super-competition also have increased eIF2α phosphorylation due to proteotoxic stress (Paul et al., 2024), we examined p-eIF2α levels in regenerating discs to determine which type of cell competition was occurring.

In an undamaged wing disc eIF2α was phosphorylated throughout the disc (Fig. 7A). After tissue damage, phosphorylation of eIF2α was reduced in the Wg+ zone of the regeneration blastema (Fig. 7B-B'). Therefore, the enhanced translation in the blastema did not cause proteotoxic stress, and the regenerating disc may be experiencing something closer to cell competition and not super-competition.

Cell elimination due to cell competition can involve an increase in autophagy (Nagata et al., 2019). Therefore, we used the autophagy marker *Atg8a-mcherry* (Hegedűs et al., 2016; Mauvezin et al., 2014) and counted mCherry-positive puncta in the cells directly adjacent to the Wg+ zone (the boundary) and in the cells within the eight-cell perimeter outside of the Wg+ zone (Fig. 7C-E). While there were few or no mCherry-positive puncta in undamaged wing discs (Fig. 7C), mCherry-positive puncta were observed in regenerating wing discs (Fig. 7D), particularly at the boundary and in the cells within the 8-cell perimeter outside of the Wg+ zone (Fig. 7E).

Xrp1 is a basic leucine zipper domain (bZIP) protein that is expressed in loser cells and is essential for loser cell elimination during imaginal disc cell competition (Baillon et al., 2018; Kiparaki et al., 2022; Lee et al., 2018; Ochi et al., 2021). We did not detect expression level differences between the cells inside the blastema and the cells

surrounding the blastema using an Xrp1 antibody (Brown et al., 2021) (Fig. 7F-G) an *Xrp1-GFP* in which the Xrp1 protein is tagged with GFP (Fig. S6A-A")(Kudron et al., 2018), or an enhancer trap line *Xrp1-lacZ*^{02515} (Bellen et al., 2004). (Fig. 7H-I). Therefore, the cell death surrounding the high Myc area in the blastema might not be mediated through *Xrp1*.

To confirm that cell death surrounding the high-Myc area is not mediated by *Xrp1*, we examined cell death in regenerating wing discs that were heterozygous for the mutant *Xrp1*$^{m2\text{-}73}$, which is a truncated allele that eliminates cell competition when heterozygous (Lee et al., 2016; Lee et al., 2018). Cell death surrounding the Wg+ blastema zone was not reduced in *Xrp1*$^{m2\text{-}73}$/+ discs (Fig. 7J-K). Given that Xrp1 is not differentially expressed, and that heterozygous *Xrp1* does not rescue the cell death at the periphery of the blastema, it is unlikely that Xrp-1 mediates this Myc-induced cell death.

The data above suggested that increased Myc in the regeneration blastema led to something closer to cell competition than super-competition. Additionally, Myc-induced cell death outside the high-Myc zone is not identical to canonical cell competition, which is mediated by Xrp1. Therefore, we conclude that the cell death seen around the Wg+, high-Myc blastema zone does not fall neatly into either the classic cell competition or super-competition categories.

Discussion

We have shown that Myc and Tor are two critical factors that regulate regenerative growth. Reduction of either Myc expression or Tor kinase activity impaired proliferation and translation in the regeneration blastema. Furthermore, our findings revealed concentric growth zones that extend beyond the blastema as defined by transcriptional profiling. We also demonstrated that the upregulated Myc expression induces cell competition-like cell death in the surrounding cells.

In our concentric growth zone model, the growth zones were differentiated through expression of genes such as Wg and Myc, activated Tor signaling, and elevated translation. Given that the shape of each zone is similar, it is likely that some secreted

factor in Growth Zone A establishes the outer zones, perhaps through damage-response signaling such as reactive oxygen species, morphogen signaling such as Wg, or mechanical signaling such as the Hippo pathway. Furthermore, the high translation in Zone C may be a non-autonomous effect of high Tor activity in Zone B. Given that these distinct zones were not identified by scRNA-seq experiments (Floc'hlay et al., 2023; Worley et al., 2022), it is unlikely that cells in Zones B and C have differential gene expression. Importantly, the differences in proliferation across the zones indicate that their underlying biological differences impact their contribution to regeneration.

Interestingly, the enhanced Myc expression in the regeneration blastema has a double-edged effect on the regenerating wing disc. While Myc drives regrowth in Growth Zone A, it also induces cell death in the neighboring cells, which includes Growth Zones B and C, tempering their ability to contribute to the regenerated tissue. Although this cell death was mediated by Myc, with proteotoxic stress reduced in the winner cells and autophagy increased in the loser cells, the loser cells did not upregulate Xrp1. Thus, these interactions did not completely resemble cell competition as described in previous studies. Notably, while Growth Zone A cells had high Myc expression and thus were winner cells, the cells outside of Growth Zone A still had elevated translation. In addition, JAK/STAT signaling was also high outside of growth Zone A, and JAK/STAT signaling can both induce cell competition and recue loser cell death (Rodrigues et al., 2012). Furthermore, JNK signaling, Yki activity, and mechanical stress can also influence cell competition (Baker, 2020; Morata, 2021). Indeed, regeneration occurs in a more complex signaling milieu than classical cell competition experiments and may provide clues to how cell competition operates in other complex microenvironments such as tumors. Furthermore, our work presents the first evidence of endogenous cell competition in a non-stem cell-based regeneration model, further exploration of which will enhance our understanding of both regeneration and cell competition.

Materials and Method

Tissue ablation

Ablation experiments were performed as previously described (Smith-Bolton et al., 2009). Briefly, egg lays were performed at 25°C in the dark for 4 hours, then incubated at 18°C. First-instar larvae were picked on day 2 and placed in vials, 50 larvae/vial. On day 7, vials were incubated for 24 hours in a 30°C circulating water bath, kept on ice for 5 minutes to reduce the temperature, then returned to the 18°C incubator Myc^{P0} animals had ablation induced 4 hours later to coincide with the early third instar stage because they have delayed development (Abidi et al., 2023).

Drosophila strains

Fly lines used were: w^{1118} (Hazelrigg et al., 1984); w^{1118}*; rnGal4*, *UAS-rpr*, *tubGal80ts/TM6B*, *tubGal80* (Smith-Bolton et al., 2009); *7xEcRE-GFP (Hackney et al., 2007; Terry et al., 2024)*(a gift from Kenneth Moberg); *Myc-lacZ* (RRID:BDSC_12247); Myc^{P0} (Johnston et al., 1999)(RRID:BDSC_11298); Tor^{2L1}(Oldham et al., 2000)(RRID:BDSC_98102); *Upd3-lacZ* (Bunker et al., 2015)(a gift from David Bilder); *10XStat92E-GFP* (Ekas et al., 2006)(RRID:BDSC_26197); Nub-*MiMIC-GFP* (*Mi{MIC}*$nub^{MI05126}$)(Venken et al., 2011a)(RRID:BDSC_37920); *UAS-Myc* (Johnston et al., 1999)(RRID:BDSC_9674); *UAS-GFP* (Shiga et al., 1996)(RRID:BDSC_4775); *Dpp-Gal4* (Kojima et al., 2000)(RRID:BDSC_93385); *Xrp1-lacZ* (Bellen et al., 2004) (RRID:BDSC_11569); *Xrp1-GFP* (Kudron et al., 2018) (RRID:BDSC_83391), $Xrp1^{M2\text{-}73}$ (Lee et al., 2018)(RRID:BDSC_81270); *3xmCherry-Atg8a (Hegedűs et al., 2016)*(a gift from Juhász Gábor).

Immunostaining

Immunostaining was carried out as previously described (Smith-Bolton et al., 2009). After dissection, the larval carcasses were fixed in 4% paraformaldehyde (PFA) for 20 minutes at room temperature, followed by 3 washes in 0.1% triton in phosphate-buffered saline (PBS) (0.1% PBST) for 10 minutes. Carcasses were incubated at 4°C overnight in primary antibodies diluted as noted below in 10% normal goat serum and 0.1% PBST, followed by 3 washes of 0.1% PBST for 10 minutes. Secondary antibody was diluted 1:1000 in 10% normal goat serum and 0.1% PBST for incubation at 4°C overnight. After the secondary antibody incubation, the samples were washed 3 times using 0.1% PBST, followed by

563 incubation in 70% glycerol in PBS overnight at 4°C. The wing imaginal discs were then
564 dissected and mounted on slides with Vectashield Anti-fade mounting media (Vector
565 Laboratories, Cat #H-1000).
566
567 Primary antibodies used: anti-Myc (1:250, Santa Cruz Biotechnologies, #sc-28207), anti-
568 p-S6 (Romero-Pozuelo et al., 2017) (1:200, a gift from Aurelio Teleman), anti-phospho-
569 Histone H3 (1:500, Millipore Sigma, #06-570), anti-Nubbin (RRID:AB_2722119) (1:250,
570 Developmental Studies Hybridoma Bank (DSHB), #Nub2D4), anti-Wingless
571 (RRID:AB_528512) (1:100, DSHB, #4D4), anti-Zfh2 (Tran et al., 2010) (1:250, a gift from
572 Chris Doe), anti-β-Galactosidase (1:500, Invitrogen, Thermo Fisher Scientific #A-11132),
573 anti-p-eIF2α (1:100, Cell Signaling, #3398), anti-Xrp1 (Brown et al., 2021) (1:1000, a gift
574 from Hyung Don Ryoo), anti-Fibrillarin (1:100, Abcam, #ab4566). Secondary antibodies
575 were Alexa Fluor 488, 555, 633, 647 (1:1000, Invitrogen) and DAPI (1:1000, Thermo
576 Fisher Scientific #D1306).
577
578 **OPP assay**
579 The OPP assay was conducted as described (Kiparaki and Baker, 2023), using the Click-
580 iT Plus OPP Alexa Fluor 488 Protein Synthesis Assay Kit (Thermo Fisher Scientific,
581 #10456). Briefly, larvae were dissected in Schneider's *Drosophila* Medium (Thermo
582 Fisher Scientific, Cat #21720024) with 10% heat-inactivated fetal bovine serum (Thermo
583 Fisher Scientific, Cat #A3840001). Larval carcasses were incubated with component A at
584 the concentration of 10 μM in Schneider's *Drosophila* Medium with 10% heat-inactivated
585 fetal bovine serum for 15 minutes. After rinsing with PBS, the carcasses were fixed in 4%
586 PFA for 20 minutes, followed by 3 washes for 10 minutes each with 0.1% PBST. After
587 washing, carcasses were blocked in 3% bovine serum albumin (BSA) in PBS for 10
588 minutes before the 30 minutes incubation in the cocktail solution for the click-on reaction.
589 After the reaction, samples were washed with the rinse buffer followed by 2 minutes of
590 blocking in 3% BSA in PBS. Protocols after this step followed the general primary and
591 secondary staining method above.
592
593 **EdU incorporation and detection**

EdU incorporation and detection was carried out as previously described (Gouge and T.W. Christensen, 2010) using the Click-iT EdU kit (Invitrogen, #C10338). Briefly, larvae were dissected in PBS and incubated in EdU at the concentration of 100 µM in Schneider's *Drosophila* Medium for 30 minutes at room temperature, followed by fixation in 4% PFA for 20 minutes, followed by 3 washes of 10 minutes each with 0.1% PBST. After washing, carcasses were blocked in 3% BSA in PBS for 30 minutes before the 30-minute incubation in the cocktail solution for the click-on reaction. Protocols after this step followed the general primary and secondary staining method above.

TUNEL assay

The TUNEL assay was carried out using the *In Situ* Cell Death Detection Kit (Roche, #12156792910). For experiments incorporating the TUNEL assay, we followed the general immunostaining protocol described above. However, for the secondary antibody solution, we used the TUNEL reaction mixture made by mixing the Enzyme Solution and Label Solution at a 1:9 ratio. Secondary antibodies and DAPI were added according to the dilutions listed above. Samples were incubated in this mixture at 4°C overnight, followed by the remainder of the protocol for general immunostaining.

Rapamycin food

Rapamycin (Thermo Fisher Scientific, #AAJ62473MC) was dissolved in ethanol at a 50 mM concentration. The rapamycin solution was added to Nutri-Fly Bloomington food (Genesee Scientific #66-121) to make a 20µM working concentration. For control food, the same amount of ethanol was added. Immediately after the temperature shift in the circulating water bath, larvae were transferred to rapamycin food or control food.

Image acquisition

Discs were imaged on a Zeiss LSM 700, Zeiss LSM 880, or Zeiss LSM 900 confocal microscope. All images for a given experiment were acquired on the same microscope with the same instrument settings. Images were processed using ImageJ (NIH). Maximum intensity projections were created for the confocal images.

Nucleolus measurements

10 nucleoli (anti-Fibrillarin staining) were measured in a 200-pixel x 200-pixel square using ImageJ.

Intensity plots

Intensity plots were made using ImageJ. Briefly, a line across the area of interest was selected using the line selection tool, then an intensity plot was generated using the Plot Profile tool.

Statistical analysis

All statistical analyses were performed using Welch's t-test on Graphpad Prism. Graphs were made on Graphpad Prism.

Acknowledgments

The authors would like to thank Anish Bose, Snigdha Mathure, and Connor Powers for critical reading of the manuscript and helpful discussions. We thank Dr. Kenneth Moberg, Dr. David Bilder, Dr. Chris Doe, Dr. Hyung Don Ryoo, Dr. Aurelio Teleman, and Dr. Juhász Gábor for reagents; the Bloomington Drosophila Stock Center (NIH P40OD018537); the Developmental Studies Hybridoma Bank (NICHD, The University of Iowa); Dr. Glenn Fried, Dr. Duncan Nall, Dr. Umnia Doha, and all the staff at Core Facilities Microscopy suite at the Carl R. Woese Institute for Genomic Biology.

Footnotes

Author contributions

F.T.-Y.H designed, carried out, interpreted the experiments, and prepared the manuscript. R.K.S.-B. designed and interpreted experiments and assisted in preparation of the manuscript.

Funding

This work was supported by the National Institutes of Health grants R01GM107140 and R35GM14174 to R.K.S.-B.

Competing interests

The authors declare no competing or financial interests.

Data and resource availability

All relevant data and resource can be found within the article and its supplementary information. In addition, raw data will be posted in the Illinois Databank (insert URL upon acceptance for publication).

Abbott, L. C., Karpen, G. H. and Schubiger, G. (1981). Compartmental restrictions and blastema formation during pattern regulation in Drosophila imaginal leg discs. *Dev Biol* **87**, 64–75.

Abidi, S. N. F., Hsu, F. T.-Y. and Smith-Bolton, R. K. (2023). Regenerative growth is constrained by brain tumor to ensure proper patterning in Drosophila. *PLoS Genet* **19**, e1011103.

Alpar, L., Bergantiños, C. and Johnston, L. A. (2018). Spatially Restricted Regulation of Spätzle/Toll Signaling during Cell Competition. *Dev Cell* **46**, 706-719.e5.

Amoyel, M. and Bach, E. A. (2014). Cell competition: How to eliminate your neighbours. *Development (Cambridge)* **141**, 988–1000.

Ascanelli, C., Dahir, R. and Wilson, C. H. (2024). Manipulating Myc for reparative regeneration. *Front Cell Dev Biol* **12**,.

Baillon, L., Germani, F., Rockel, C., Hilchenbach, J. and Basler, K. (2018). Xrp1 is a transcription factor required for cell competition-driven elimination of loser cells. *Sci Rep* **8**, 17712.

Baker, N. E. (2020). Emerging mechanisms of cell competition. *Nat Rev Genet* **21**, 683–697.

Baumgartner, M. E., Dinan, M. P., Langton, P. F., Kucinski, I. and Piddini, E. (2021). Proteotoxic stress is a driver of the loser status and cell competition. *Nat Cell Biol* **23**, 136–146.

Bawa, S., Brooks, D. S., Neville, K. E., Tipping, M., Sagar, M. A., Kollhoff, J. A., Chawla, G., Geisbrecht, B. V, Tennessen, J. M., Eliceiri, K. W., et al. (2020). Drosophila TRIM32 cooperates with glycolytic enzymes to promote cell growth. *Elife* **9**,.

Bellen, H. J., Levis, R. W., Liao, G., He, Y., Carlson, J. W., Tsang, G., Evans-Holm, M., Hiesinger, P. R., Schulze, K. L., Rubin, G. M., et al. (2004). The BDGP Gene Disruption Project. *Genetics* **167**, 761–781.

Bellosta, P. and Gallant, P. (2010). Myc Function in Drosophila. *Genes Cancer* **1**, 542–546.

Bergantiños, C., Corominas, M. and Serras, F. (2010). Cell death-induced regeneration in wing imaginal discs requires JNK signalling. *Development* **137**, 1169–1179.

Blanco, J., Cooper, J. C. and Baker, N. E. (2020). Roles of C/EBP class bZip proteins in the growth and cell competition of Rp ('Minute') mutants in Drosophila. *Elife* **9**,.

Bosch, M., Serras, F., Martín-Blanco, E. and Baguñà, J. (2005). JNK signaling pathway required for wound healing in regenerating Drosophila wing imaginal discs. *Dev Biol* **280**, 73–86.

Bosch, M., Bagun, J. and Serras, F. (2008). Origin and proliferation of blastema cells during regeneration of Drosophila wing imaginal discs. *Int J Dev Biol* **52**, 1043–1050.

Brandão, A. S., Borbinha, J., Pereira, T., Brito, P. H., Lourenço, R., Bensimon-Brito, A. and Jacinto, A. (2022). A regeneration-triggered metabolic adaptation is necessary for cell identity transitions and cell cycle re-entry to support blastema formation and bone regeneration. *Elife* **11**,.

Brown, B., Mitra, S., Roach, F. D., Vasudevan, D. and Ryoo, H. D. (2021). The transcription factor Xrp1 is required for PERK-mediated antioxidant gene induction in Drosophila. *Elife* **10**,.

Bunker, B. D., Nellimoottil, T. T., Boileau, R. M., Classen, A. K. and Bilder, D. (2015). The transcriptional response to tumorigenic polarity loss in Drosophila. *Elife* **4**,.

Colombani, J., Andersen, D. S. and Léopol, P. (2012). Secreted peptide dilp8 coordinates Drosophila tissue growth with developmental timing. *Science (1979)* **336**, 582–585.

De La Cova, C., Abril, M., Bellosta, P., Gallant, P. and Johnston, L. A. (2004). Drosophila myc regulates organ size by inducing cell competition. *Cell* **117**, 107–116.

De La Cova, C., Senoo-Matsuda, N., Ziosi, M., Wu, D. C., Bellosta, P., Quinzii, C. M. and Johnston, L. A. (2014). Supercompetitor status of drosophila Myc cells requires p53 as a Fitness sensor to reprogram metabolism and promote viability. *Cell Metab* **19**, 470–483.

Ekas, L. A., Baeg, G.-H., Flaherty, M. S., Ayala-Camargo, A. and Bach, E. A. (2006). JAK/STAT signaling promotes regional specification by negatively regulating *wingless* expression in *Drosophila*. *Development* **133**, 4721–4729.

Floc'hlay, S., Balaji, R., Stanković, D., Christiaens, V. M., Bravo González-Blas, C., De Winter, S., Hulselmans, G. J., De Waegeneer, M., Quan, X., Koldere, D., et al. (2023). Shared enhancer gene regulatory networks between wound and oncogenic programs. *Elife* **12**,.

Fox, D. T., Cohen, E. and Smith-Bolton, R. (2020). Model systems for regeneration: *Drosophila*. *Development* **147**,.

Garelli, A., Gontijo, A. M., Miguela, V., Caparros, E. and Dominguez, M. (2012). Imaginal discs secrete insulin-like peptide 8 to mediate plasticity of growth and maturation. *Science (1979)* **336**, 579–582.

Germani, F., Hain, D., Sternlicht, D., Moreno, E. and Basler, K. (2018). The Toll pathway inhibits tissue growth and regulates cell fitness in an infection-dependent manner. *Elife* **7**,.

Gouge, C. A. and T.W. Christensen (2010). Technique Notes-Detection of S Phase in multiple Drosophila tissues utiliizing the EdU labeling technique. *Drosoph Inf Serv* **93**, 203.

Grewal, S. S., Li, L., Orian, A., Eisenman, R. N. and Edgar, B. A. (2005). Myc-dependent regulation of ribosomal RNA synthesis during Drosophila development. *Nat Cell Biol* **7**, 295–302.

Grusche, F. A., Degoutin, J. L., Richardson, H. E. and Harvey, K. F. (2011). The Salvador/Warts/Hippo pathway controls regenerative tissue growth in Drosophila melanogaster. *Dev Biol* **350**, 255–266.

Hackney, J. F., Pucci, C., Naes, E. and Dobens, L. (2007). Ras signaling modulates activity of the ecdysone receptor EcR during cell migration in the drosophila ovary. *Developmental Dynamics* **236**, 1213–1226.

Hadorn, E. and Buck, D. (1962). Über entwicklungsleistungen transplantierter teilstücke von flügel-imaginalscheiben von Drosophila melanogaster. *Revue suisse de Zoologie*.

Halme, A., Cheng, M. and Hariharan, I. K. (2010). Retinoids Regulate a Developmental Checkpoint for Tissue Regeneration in Drosophila. *Current Biology* **20**, 458–463.

Harris, R. E., Setiawan, L., Saul, J. and Hariharan, I. K. (2016). Localized epigenetic silencing of a damage-activated WNT enhancer limits regeneration in mature Drosophila imaginal discs. *Elife* **5**,.

Harris, R. E., Stinchfield, M. J., Nystrom, S. L., McKay, D. J. and Hariharan, I. K. (2020). Damage-responsive, maturity-silenced enhancers regulate multiple genes that direct regeneration in drosophila. *Elife* **9**, 1–26.

Hazelrigg, T., Levis, R. and Rubin, G. M. (1984). Transformation of white locus DNA in Drosophila: Dosage compensation, zeste interaction, and position effects. *Cell* **36**, 469–481.

Hegedűs, K., Takáts, S., Boda, A., Jipa, A., Nagy, P., Varga, K., Kovács, A. L. and Juhász, G. (2016). The Ccz1-Mon1-Rab7 module and Rab5 control distinct steps of autophagy. *Mol Biol Cell* **27**, 3132–3142.

Herrera, S. C., Martín, R. and Morata, G. (2013). Tissue Homeostasis in the Wing Disc of Drosophila melanogaster: Immediate Response to Massive Damage during Development. *PLoS Genet* **9**, e1003446.

Jaszczak, J. S. and Halme, A. (2016). Arrested development: coordinating regeneration with development and growth in Drosophila melanogaster. *Curr Opin Genet Dev* **40**, 87–94.

Jaszczak, J. S., Wolpe, J. B., Dao, A. Q. and Halme, A. (2015). Nitric Oxide Synthase Regulates Growth Coordination During *Drosophila melanogaster* Imaginal Disc Regeneration. *Genetics* **200**, 1219–1228.

Jaszczak, J. S., Wolpe, J. B., Bhandari, R., Jaszczak, R. G. and Halme, A. (2016). Growth Coordination During *Drosophila melanogaster* Imaginal Disc Regeneration Is Mediated by Signaling Through the Relaxin Receptor Lgr3 in the Prothoracic Gland. *Genetics* **204**, 703–709.

Johnston, L. A., Prober, D. A., Edgar, B. A., Eisenman, R. N. and Gallant, P. (1999). Drosophila myc regulates cellular growth during development. *Cell* **98**, 779–790.

Karanja, F., Sahu, S., Weintraub, S., Bhandari, R., Jaszczak, R., Sitt, J. and Halme, A. (2022). Ecdysone exerts biphasic control of regenerative signaling, coordinating the completion of regeneration with developmental progression. *Proceedings of the National Academy of Sciences* **119**,.

Katsuyama, T., Comoglio, F., Seimiya, M., Cabuy, E. and Paro, R. (2015). During *Drosophila* disc regeneration, JAK/STAT coordinates cell proliferation with Dilp8-mediated developmental delay. *Proceedings of the National Academy of Sciences* **112**,.

Khan, S. J., Abidi, S. N. F., Skinner, A., Tian, Y. and Smith-Bolton, R. K. (2017). *The Drosophila Duox maturation factor is a key component of a positive feedback loop that sustains regeneration signaling*.

Khandekar, A. and Ellis, S. J. (2024). An expanded view of cell competition. *Development* **151**,.

Kiparaki, M. and Baker, N. E. (2023). Protocol for assessing translation in living Drosophila imaginal discs by O-propargyl-puromycin incorporation. *STAR Protoc* **4**, 102653.

Kiparaki, M., Khan, C., Folgado-Marco, V., Chuen, J., Moulos, P. and Baker, N. E. (2022). The transcription factor Xrp1 orchestrates both reduced translation and cell competition upon defective ribosome assembly or function. *Elife* **11**,.

Kojima, T., Sato, M. and Saigo, K. (2000). Formation and specification of distal leg segments in *Drosophila* by dual *Bar* homeobox genes, *BarH1* and *BarH2*. *Development* **127**, 769–778.

Kudron, M. M., Victorsen, A., Gevirtzman, L., Hillier, L. W., Fisher, W. W., Vafeados, D., Kirkey, M., Hammonds, A. S., Gersch, J., Ammouri, H., et al. (2018). The ModERN Resource: Genome-Wide Binding Profiles for Hundreds of *Drosophila* and *Caenorhabditis elegans* Transcription Factors. *Genetics* **208**, 937–949.

Kuo, Y., Huang, H., Cai, T. and Wang, T. (2015). Target of rapamycin complex 2 regulates cell growth via Myc in drosophila. *Sci Rep* **5**, 1–10.

Ledru, M., Clark, C. A., Brown, J., Verghese, S., Ferrara, S., Goodspeed, A. and Su, T. T. (2022). Differential gene expression analysis identified determinants of cell fate plasticity during radiation-induced regeneration in Drosophila. *PLoS Genet* **18**, e1009989.

Lee, C.-H., Rimesso, G., Reynolds, D. M., Cai, J. and Baker, N. E. (2016). Whole-Genome Sequencing and iPLEX MassARRAY Genotyping Map an EMS-Induced Mutation Affecting Cell Competition in *Drosophila melanogaster*. *G3 Genes|Genomes|Genetics* **6**, 3207–3217.

Lee, C.-H., Kiparaki, M., Blanco, J., Folgado, V., Ji, Z., Kumar, A., Rimesso, G. and Baker, N. E. (2018). A Regulatory Response to Ribosomal Protein Mutations Controls Translation, Growth, and Cell Competition. *Dev Cell* **46**, 456-469.e4.

Li, W. and Baker, N. E. (2007). Engulfment Is Required for Cell Competition. *Cell* **129**, 1215–1225.

Londono, R., Sun, A. X., Tuan, R. S. and Lozito, T. P. (2018). Tissue Repair and Epimorphic Regeneration: an Overview. *Curr Pathobiol Rep* **6**, 61–69.

Mauvezin, C., Ayala, C., Braden, C. R., Kim, J. and Neufeld, T. P. (2014). Assays to monitor autophagy in Drosophila. *Methods* **68**, 134–139.

Merino, M. M., Rhiner, C., Lopez-Gay, J. M., Buechel, D., Hauert, B. and Moreno, E. (2015). Elimination of Unfit Cells Maintains Tissue Health and Prolongs Lifespan. *Cell* **160**, 461–476.

Meyer, S. N., Amoyel, M., Bergantiños, C., De La Cova, C., Schertel, C., Basler, K. and Johnston, L. A. (2014). An ancient defense system eliminates unfit cells from developing tissues during cell competition. *Science (1979)* **346**,.

Morata, G. (2021). Cell competition: A historical perspective. *Dev Biol* **476**, 33–40.

Nagata, R., Nakamura, M., Sanaki, Y. and Igaki, T. (2019). Cell Competition Is Driven by Autophagy. *Dev Cell* **51**, 99-112.e4.

Ng, M., Diaz-Benjumea, F. J. and Cohen, S. M. (1995). *nubbin* encodes a POU-domain protein required for proximal-distal patterning in the *Drosophila* wing. *Development* **121**, 589–599.

O'Brochta, D. A. and Bryant, P. J. (1987). Distribution of S-phase cells during the regeneration of Drosophila imaginal wing discs. *Dev Biol* **119**, 137–142.

Ochi, N., Nakamura, M., Nagata, R., Wakasa, N., Nakano, R. and Igaki, T. (2021). Cell competition is driven by Xrp1-mediated phosphorylation of eukaryotic initiation factor 2α. *PLoS Genet* **17**, e1009958.

Oldham, S., Montagne, J., Radimerski, T., Thomas, G. and Hafen, E. (2000). Genetic and biochemical characterization of dTOR, the *Drosophila* homolog of the target of rapamycin. *Genes Dev* **14**, 2689–2694.

Parisi, F., Riccardo, S., Daniel, M., Saqcena, M., Kundu, N., Pession, A., Grifoni, D., Stocker, H., Tabak, E. and Bellosta, P. (2011). Drosophila insulin and target of rapamycin (TOR) pathways regulate GSK3 beta activity to control Myc stability and determine Myc expression in vivo. *BMC Biol* **9**, 65.

Paul, P. K., Umarvaish, S., Bajaj, S., S., R. F., Mohan, H., Annaert, W. and Chaudhary, V. (2024). Maintenance of proteostasis by Drosophila Rer1 is essential for competitive cell survival and Myc-driven overgrowth. *PLoS Genet* **20**, e1011171.

Rai, M., Carter, S. M., Shefali, S. A., Chawla, G. and Tennessen, J. M. (2024). Characterization of genetic and molecular tools for studying the endogenous expression of Lactate dehydrogenase in Drosophila melanogaster. *PLoS One* **19**, e0287865.

Rhiner, C., López-Gay, J. M., Soldini, D., Casas-Tinto, S., Martín, F. A., Lombardía, L. and Moreno, E. (2010). Flower forms an extracellular code that reveals the fitness of a cell to its neighbors in Drosophila. *Dev Cell* **18**, 985–998.

Rodrigues, A. B., Zoranovic, T., Ayala-Camargo, A., Grewal, S., Reyes-Robles, T., Krasny, M., Christine Wu, D., Johnston, L. A. and Bach, E. A. (2012). Activated STAT regulates growth and induces competitive interactions independently of Myc, Yorkie, Wingless and ribosome biogenesis. *Development (Cambridge)* **139**, 4051–4061.

Romero-Pozuelo, J., Demetriades, C., Schroeder, P. and Teleman, A. A. (2017). CycD/Cdk4 and Discontinuities in Dpp Signaling Activate TORC1 in the Drosophila Wing Disc. *Dev Cell* **42**, 376-387.e5.

Santabárbara-Ruiz, P., López-Santillán, M., Martínez-Rodríguez, I., Binagui-Casas, A., Pérez, L., Milán, M., Corominas, M. and Serras, F. (2015). ROS-Induced JNK and p38 Signaling Is Required for Unpaired Cytokine Activation during Drosophila Regeneration. *PLoS Genet* **11**, e1005595.

Serras, F. and Bellosta, P. (2024). Drosophila: a Tale of regeneration with MYC. *Front Cell Dev Biol* **12**,.

Shiga, Y., Tanaka-Matakatsu, M. and Hayashi, S. (1996). A nuclear GFP/β-galactosidase fusion protein as a marker for morphogenesis in living *Drosophila*. *Dev Growth Differ* **38**, 99–106.

Smith-Bolton, R. K., Worley, M. I., Kanda, H. and Hariharan, I. K. (2009). Regenerative Growth in Drosophila Imaginal Discs Is Regulated by Wingless and Myc. *Dev Cell* **16**, 797–809.

Sun, G. and Irvine, K. D. (2011). Regulation of Hippo signaling by Jun kinase signaling during compensatory cell proliferation and regeneration, and in neoplastic tumors. *Dev Biol* **350**, 139–151.

Swarup, S. and Verheyen, E. M. (2012). Wnt/Wingless Signaling in Drosophila. *Cold Spring Harb Perspect Biol* **4**, a007930–a007930.

Teleman, A. A., Hietakangas, V., Sayadian, A. C. and Cohen, S. M. (2008). Nutritional Control of Protein Biosynthetic Capacity by Insulin via Myc in Drosophila. *Cell Metab* **7**, 21–32.

Terriente, J., Perea, D., Suzanne, M. and Díaz-Benjumea, F. J. (2008). The Drosophila gene zfh2 is required to establish proximal-distal domains in the wing disc. *Dev Biol* **320**, 102–112.

Terry, D., Schweibenz, C. and Moberg, K. (2024). Local Ecdysone synthesis in a wounded epithelium sustains developmental delay and promotes regeneration in *Drosophila*. *Development* **151**,.

Thummel, C. S. (2001). Molecular Mechanisms of Developmental Timing in C. elegans and Drosophila. *Dev Cell* **1**, 453–465.

Tran, K. D., Miller, M. R. and Doe, C. Q. (2010). Recombineering Hunchback identifies two conserved domains required to maintain neuroblast competence and specify early-born neuronal identity. *Development* **137**, 1421–1430.

Venken, K. J. T., Schulze, K. L., Haelterman, N. A., Pan, H., He, Y., Evans-Holm, M., Carlson, J. W., Levis, R. W., Spradling, A. C., Hoskins, R. A., et al. (2011a). MiMIC: a highly versatile transposon insertion resource for engineering Drosophila melanogaster genes. *Nat Methods* **8**, 737–43.

Venken, K. J. T., Schulze, K. L., Haelterman, N. A., Pan, H., He, Y., Evans-Holm, M., Carlson, J. W., Levis, R. W., Spradling, A. C., Hoskins, R. A., et al. (2011b). MiMIC: a highly versatile transposon insertion resource for engineering Drosophila melanogaster genes. *Nat Methods* **8**, 737–743.

Worley, M. I., Alexander, L. A. and Hariharan, I. K. (2018). CtBP impedes JNK- and Upd/STAT-driven cell fate misspecifications in regenerating Drosophila imaginal discs. *Elife* **7**,.

Worley, M. I., Everetts, N. J., Yasutomi, R., Chang, R. J., Saretha, S., Yosef, N. and Hariharan, I. K. (2022). Ets21C sustains a pro-regenerative transcriptional program in blastema cells of Drosophila imaginal discs. *Current Biology* **32**, 3350-3364.e6.

Fig.1

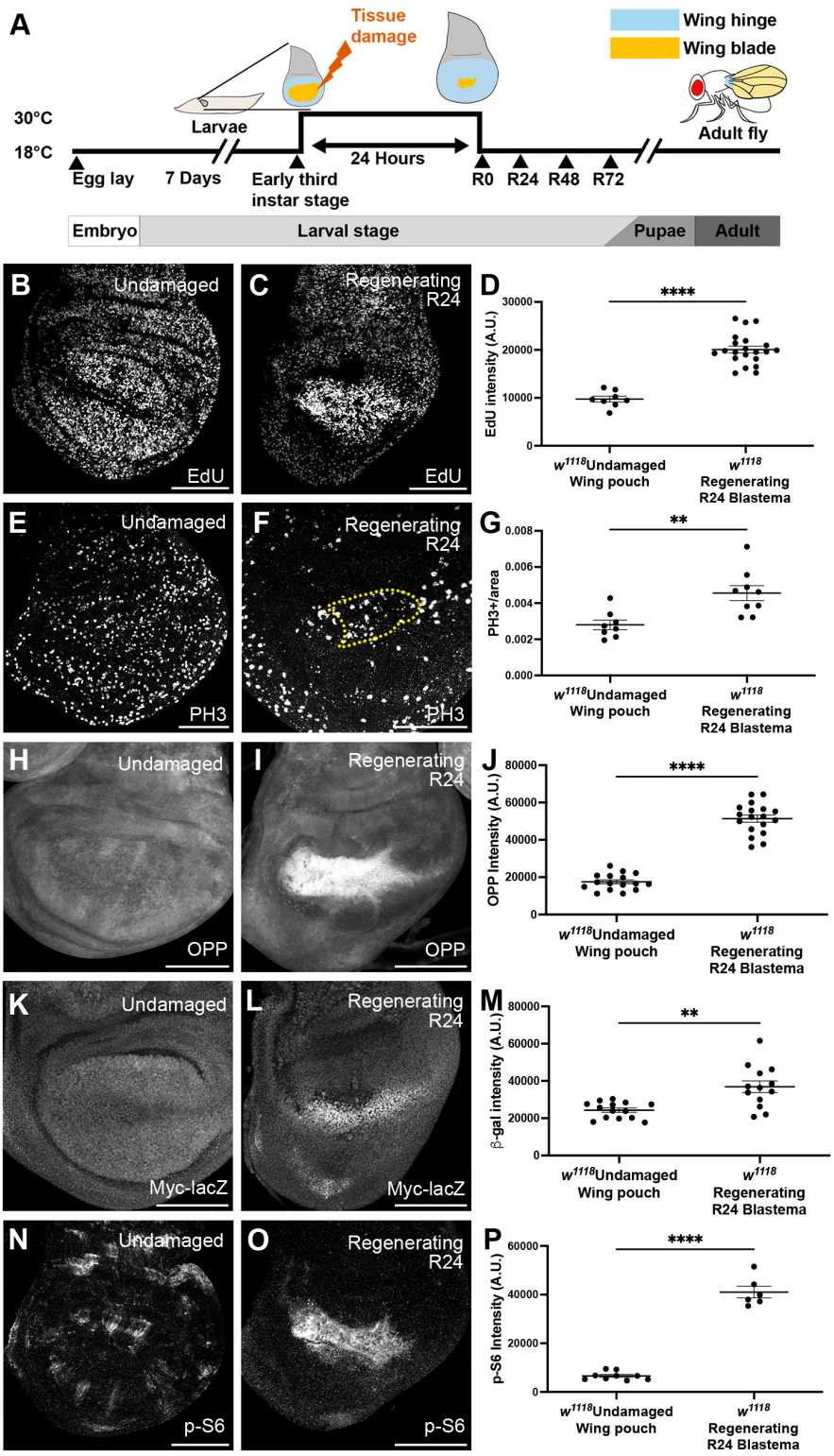

664 **Figure legends**

665 **Figure 1. Myc expression and Tor signaling in regenerating wing discs**

666 (A) Schematic of the genetic ablation system. (B-C) EdU incorporation marking S-phase
667 cells in an undamaged disc (B) and an R24 disc (C). (D) Quantification of average EdU
668 staining intensity in the wing pouch identified by morphological features. Undamaged
669 n=8, R24 n=21. ****P<0.0001. (E-F) PH3 staining marking mitotic cells in an
670 undamaged disc (E) and an R24 disc (F). (G) Quantification of mitotic cells per area in
671 the wing pouch identified by inner ring of Wg staining (yellow dotted lines in 1F).
672 Undamaged n=8, R24 n=9. **P<0.01. (H-I) OPP assay in an undamaged disc (H) and
673 an R24 disc (I). (J) Quantification of OPP staining intensity in the wing pouch of an
674 undamaged disc or blastema of an R24 disc, identified by the inner ring of Wg staining
675 or Wg staining, respectively. Undamaged n=16, R24 n=18. ****P<0.0001. (K-L) *Myc-*
676 *lacZ* expression detected by β-gal staining in an undamaged disc (K) and an R24 disc
677 (L). (M) Quantification of average β-gal staining intensity in the wing pouch or blastema
678 identified by morphological features. Undamaged n=14, R24 n=13. **P<0.01. (N-O) p-
679 S6 staining in an undamaged disc (N) and an R24 disc (O). (P) Quantification of
680 average p-S6 staining intensity in the wing pouch or blastema identified by Wg staining.
681 Undamaged n=9, R24 n=6. ****P<0.0001. Statistical test used was Welch's t-test. Scale
682 bars are 100μm. Error bars are SEM.
683

Fig. 2

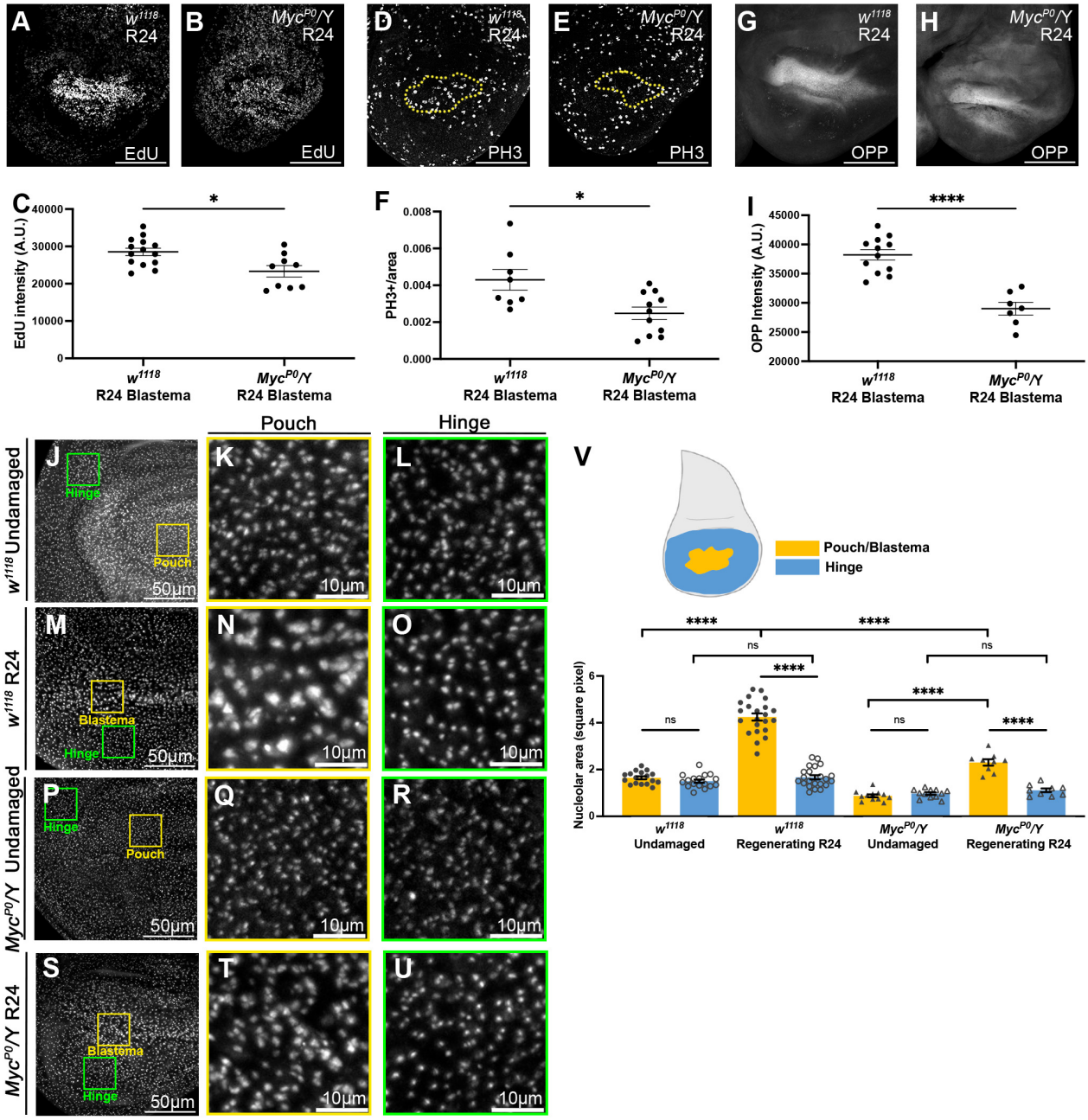

Figure 2. Myc promotes growth in the regeneration blastema

(A-B) EdU incorporation in a w^{1118} R24 disc (A) and a Myc^{P0}/Y R24 disc (B). (C) Quantification of average EdU intensity in the wing pouch identified by morphological features. w^{1118}n=14, Myc^{P0}/Y n=9. *P<0.05. (D-E) PH3 staining in a w^{1118} R24 disc (D) and a Myc^{P0}/Y R24 disc (E). (F) Quantification of mitotic cells per area in the blastema (Wg, yellow dotted lines in D-E). w^{1118} n=8, Myc^{P0}/Y n=11. *P<0.05. (G-H) OPP assay in a w^{1118} R24 disc (G) and a Myc^{P0}/Y R24 disc (H). (I) Quantification of average OPP signal in the Wg+ blastema. w^{1118} n=12, Myc^{P0}/Y n=7. ****P<0.0001. (J-U) Fibrillarin staining marking nucleoli in a w^{1118} undamaged disc (J-L), a w^{1118} R24 disc (M-O), a Myc^{P0}/Y undamaged disc (P-R), and a Myc^{P0}/Y R24 disc (S-U). (K,N,Q,T) 200-pixel square from pouch or Wg+ blastema (yellow boxes). (L,O,R,U) 200-pixel square from hinge (green boxes). (V) Quantification of nucleolus size. w^{1118} undamaged n=17, w^{1118} R24 n=22, Myc^{P0}/Y undamaged n=12, Myc^{P0}/Y R24 n=9. n.s. P>0.05, ****P<0.0001. Statistical test used was Welch's t-test. Scale bars are 100μm. Error bars are SEM.

Fig. 3

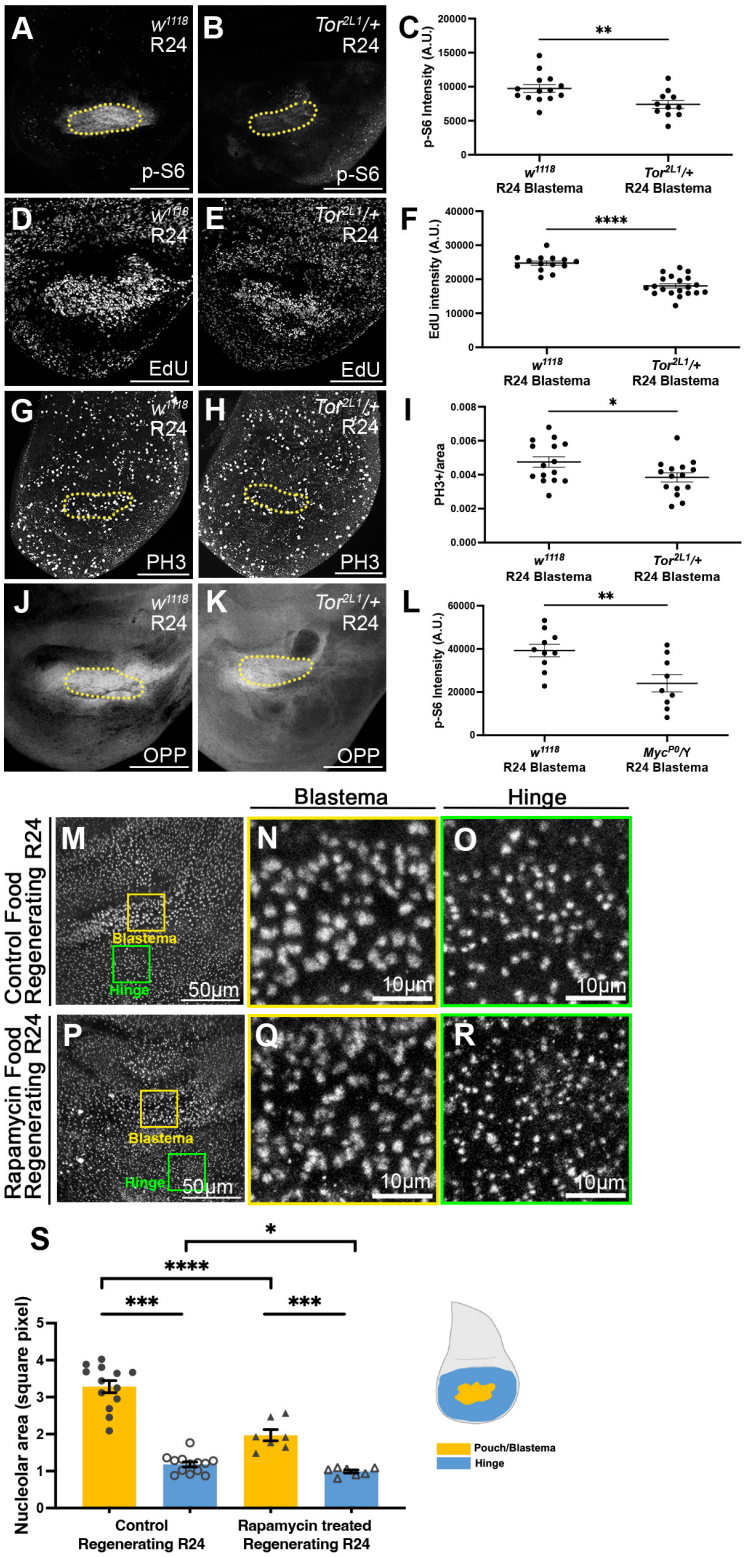

Figure 3. Tor promotes growth in the regeneration blastema

(A-B) p-S6 immunostaining in a w^{1118} R24 disc (A) and a Tor^{2L1}/+ R24 disc (B). (C) Quantification of average p-S6 staining intensity in the Wg+ blastema (yellow dotted lines). w^{1118} n=14, Tor^{2L1}/+ n=11. **P<0.01, Welch's t-test. (D-E) EdU incorporation in a w^{1118} R24 disc (D) and a Tor^{2L1}/+ R24 disc (E). (F) Quantification of average EdU staining intensity in the blastema identified by morphological features. w^{1118} n=14, Tor^{2L1}/+ n=20. ****P<0.0001. (G-H) PH3 staining in a w^{1118} R24 disc (G) and a Tor^{2L1}/+ R24 disc (H). (I) Quantification of mitotic cells per area in the Wg+ blastema (yellow dotted lines). w^{1118} n=15, Tor^{2L1}/+ n=15. *P<0.05. (J-K) OPP assay in a w^{1118} R24 disc (J) and a Tor^{2L1}/+ R24 disc (K). (L) Quantification of average OPP staining in the Wg+ blastema (yellow dotted lines). w^{1118} n=16, Tor^{2L1}/+ n=16. ***P<0.001. (M-S) Fibrillarin staining in an R24 disc after feeding with control food (M-O) or food containing rapamycin (P-R). (N,Q) 200-pixel squares from the Wg+ blastema (yellow boxes). (O,R) 200-pixel square from the hinge (green boxes). (S) Quantification of nucleolus size in hinge and blastema. control n=13, rapamycin n=7. *P<0.05, ***P<0.001, ****P<0.0001.

Fig. 4

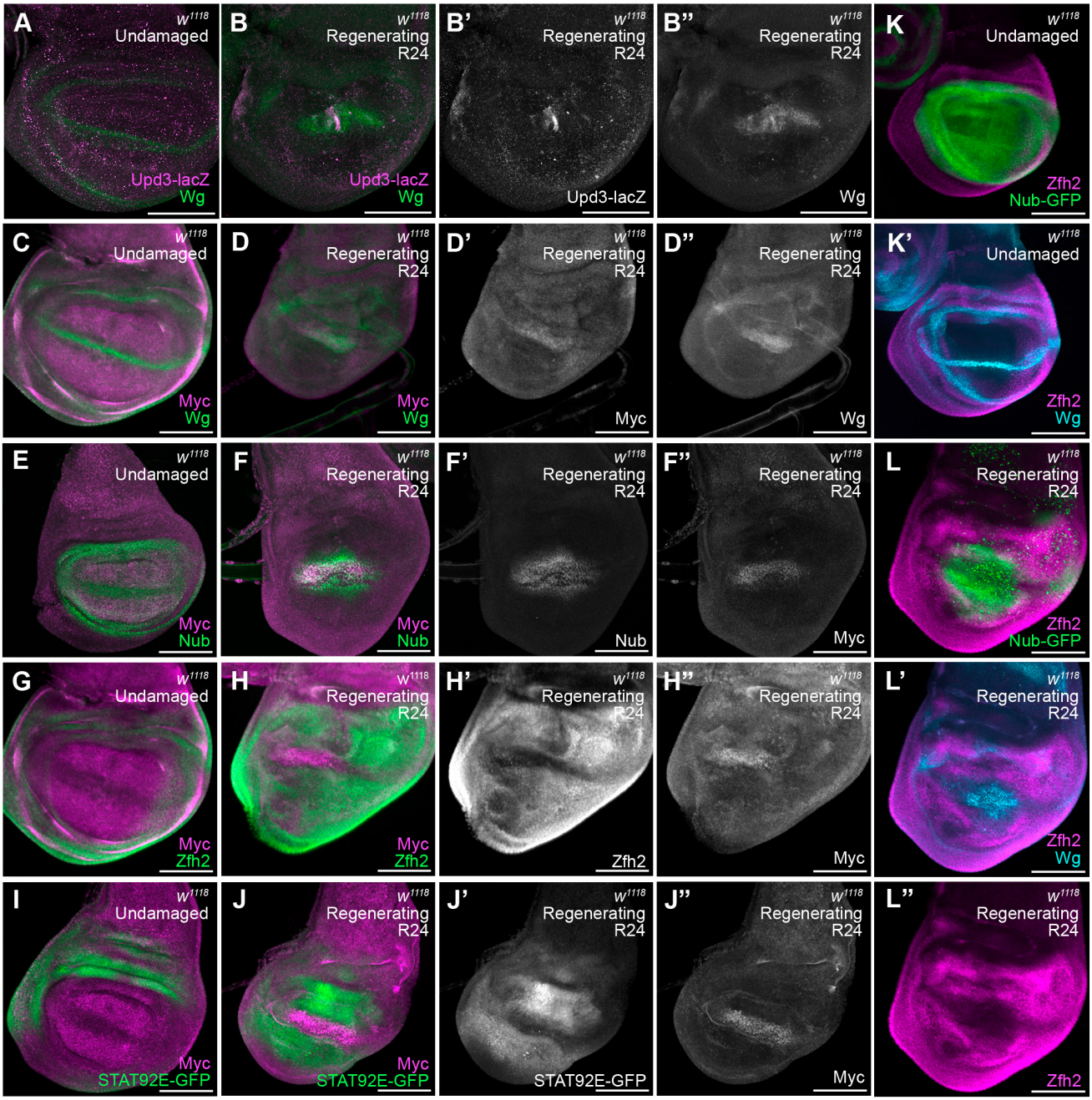

Figure 4. Mapping the domain of Myc expression in the regeneration blastema

(A-B") Wg immunostaining and *upd-lacZ* expression detected by β-Gal immunostaining in an undamaged disc (A) and an R24 disc (B-B"). (C-D") Myc and Wg immunostaining in an undamaged disc (C) and an R24 disc (D-D"). (E-F") Nub and Wg immunostaining in an undamaged disc (E) and an R24 disc (F-F"). (G-H') Zfh2 and Wg immunostaining in an undamaged disc (G) and an R24 disc (H-H"). (I-J") *STAT92E-GFP* expression and Wg staining in an undamaged disc (I) and an R24 disc (J-J"). (K-L") Zfh2 and Wg staining as well as *nub-GFP* expression in an undamaged disc (K-K') and an R24 disc (L-L"). Scale bars are 100μm.

Fig. 5

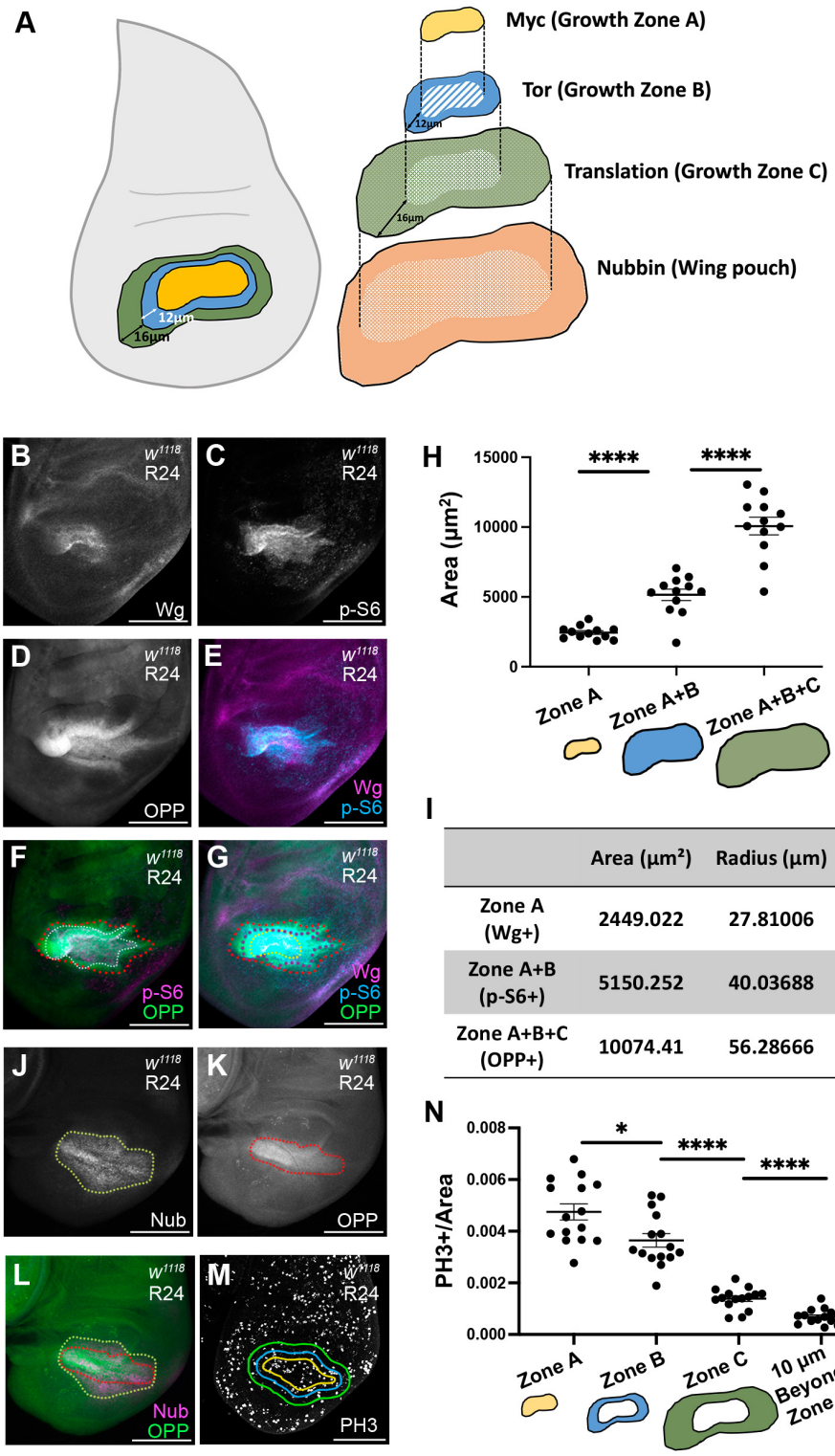

	Area (µm²)	Radius (µm)
Zone A (Wg+)	2449.022	27.81006
Zone A+B (p-S6+)	5150.252	40.03688
Zone A+B+C (OPP+)	10074.41	56.28666

728 **Figure 5. Zones of growth in the regeneration blastema**

729 (A) Schematic of concentric growth zones in a regenerating wing disc. (B-G) Wg
730 staining (yellow dashed line), p-S6 staining (white dashed line) and OPP assay (red
731 dashed line) in the same R24 disc. (B) Wg. (C) p-S6. (D) OPP assay. (E) Wg and p-S6.
732 (F) Wg and OPP assay. (G) Wg, p-S6, and OPP assay. (H) Quantification of area in
733 zones identified by Wg, p-S6, and the OPP assay. n=12. ****P<0.0001, Welch's t-test.
734 (I) Average area and radius of each zone. (J-L) R24 disc with Nub staining (J), OPP
735 assay (K), and merged image (L). (M) PH3 staining in an R24 disc. Yellow line outlines
736 Growth Zone A. Blue line outlines Growth Zone B, 13 microns beyond Growth Zone A.
737 Green line outlines Growth Zone C, 16 microns beyond Growth Zone B. (N)
738 Quantification of mitotic cells per area in each growth zone identified as in (M). n=15.
739 *P<0.05, ****P<0.0001, Welch's t-test. Scale bars are 100μm. Error bars are SEM.
740
741

Fig. 6

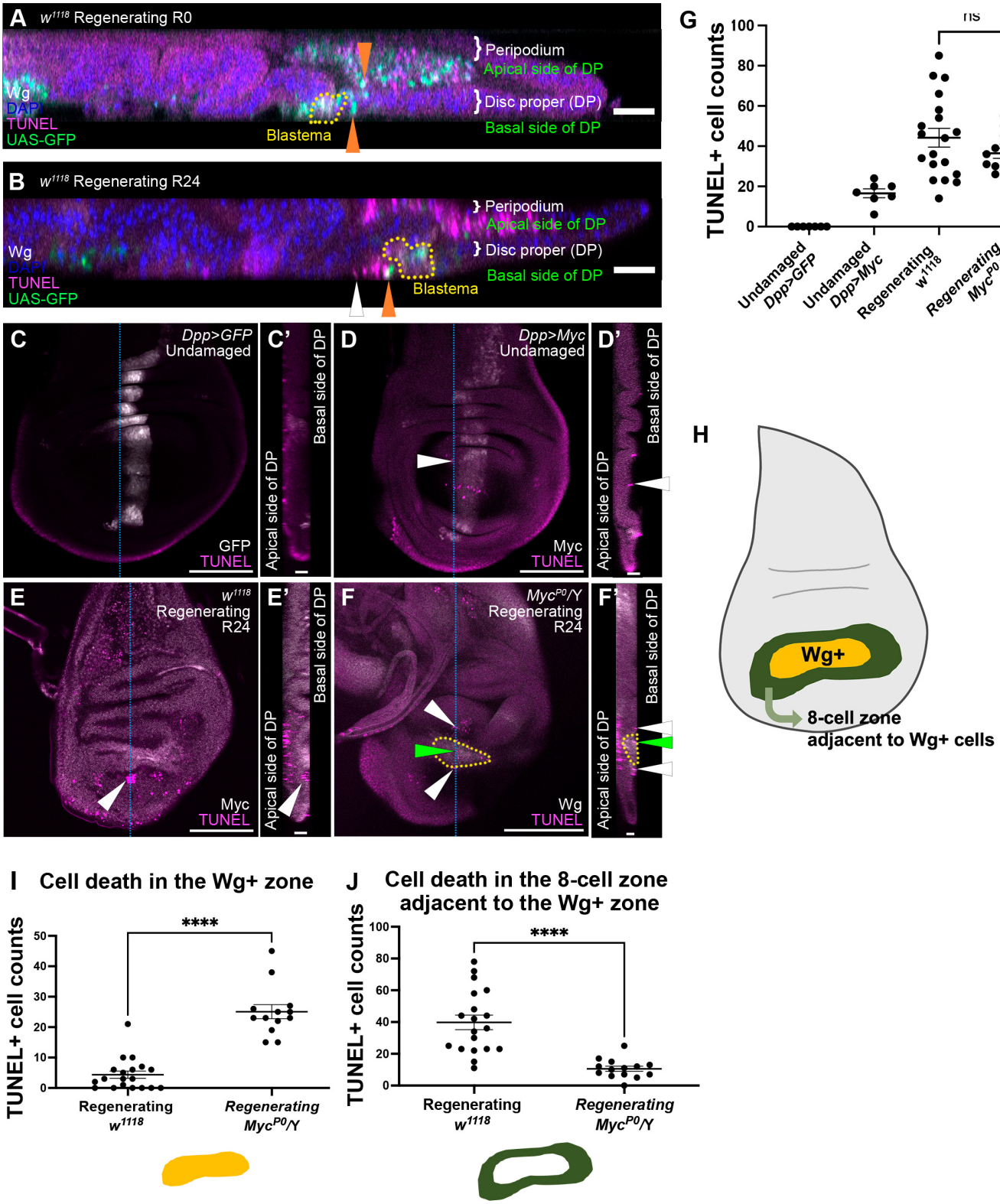

Figure 6. Myc expression induces cell death at the periphery of Growth Zone A

(A-B) Orthogonal views of an R0 disc (A) and an R24 disc (B). Wg staining (white) marks the regeneration blastema (yellow dotted lines). UAS-GFP (green) marks cell debris from tissue ablation. TUNEL assay (magenta) marks debris and apoptotic cells. DAPI (blue) marks nuclei. White arrowhead marks TUNEL+ GFP- apoptotic cell, orange arrowhead marks TUNEL+ GFP+ cell debris. (C-F) TUNEL assay marking apoptotic cells in a negative control (*dpp-Gal4>UASGFP*) (C), positive control (*dppGal4>UASMyc*) (D), w^{1118} R24 disc (E), and Myc^{P0}/Y R24 disc (F). (E) w^{1118} R24 disc with Myc staining marking Growth Zone A. (F) Myc^{P0}/Y R24 disc with Wg staining (yellow line) marking Growth Zone A. (C',D',E',F') Orthogonal views of (C,D,E,F). White arrowheads mark apoptosis adjacent to high Myc expression. Green arrowhead marks apoptosis in the blastema. (G) Quantification of cell death labeled by TUNEL at the basal side of the epithelium in the areas that were GFP+ (C) or Myc+ (D) in the wing pouch and an eight-cell band extending anteriorly, or the Wg+ Myc+ blastema and an eight-cell band outside of the blastema. *dpp>GFP* n=7, *dpp>Myc* n=7, w^{1118} R24 n=19, Myc^{P0}/Y R24 n=14. n.s. P>0.05, Welch's t-test. (H) Schematic of a regenerating wing disc, yellow indicates the Wg+Myc+ zone, green indicates the eight cells beyond. (I) Quantification of cell death in the Wg+ zone in R24 discs. w^{1118} n=19, Myc^{P0}/Y n=14. ****P<0.0001, Welch's t-test. (J) Quantification of cell death in the eight-cell band outside the Wg+ zone. w^{1118} n=19, Myc^{P0}/Y n=14. ****P<0.0001, Welch's t-test. Scale bars are 100μm. Error bars are SEM.

Fig. 7

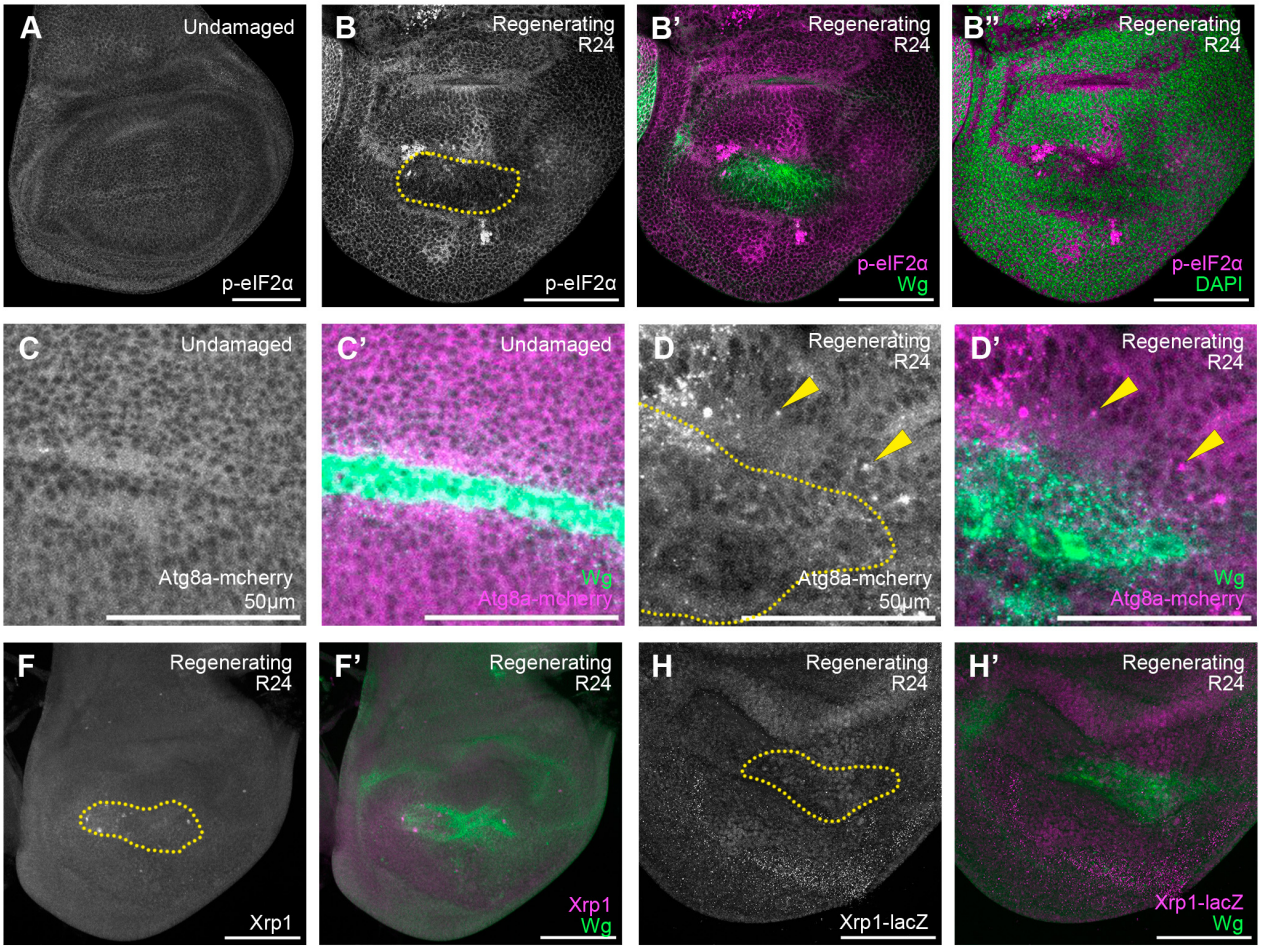

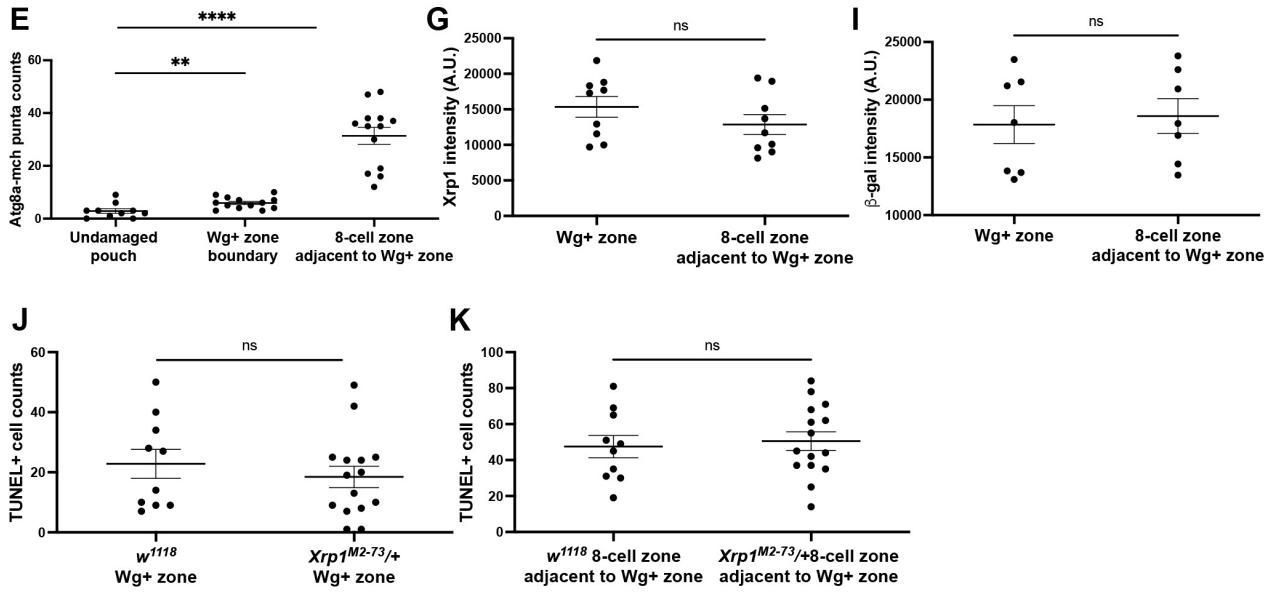

765 **Figure 7. Cell competition induced in regenerating wing discs is distinct from**
766 **experimentally induced cell competition**
767 (A-B) p-eIF2α staining in an undamaged disc (A) and an R24 disc (B). (B') p-eIF2α and
768 Wg. (B") p-eIF2α and DAPI. (C-D) Atg8a-mcherry expression in an undamaged disc (C)
769 and an R24 disc (D). (C'-D') Atg8a-mcherry expression and Wg staining (yellow circle).
770 Arrowheads indicate Atg8a puncta. (E) Quantification of Atg8a puncta. n=13. **P<0.01,
771 ****P<0.0001. (F-F') Xrp1 staining in an R24 disc. Yellow dotted circle indicates
772 blastema marked by Wg. (G) Quantification of Xrp1 intensity. n=9, n.s. P>0.05. (H-H')
773 *Xrp1-lacZ* expression in an R24 disc. Yellow dotted circle indicates blastema marked by
774 Wg. (I) Quantification of average β-gal staining intensity. n=7, n.s. P>0.05. (J-K)
775 Quantification of cell death (TUNEL) in the Wg+ area (J) and in the 8-cell zone adjacent
776 to the Wg+ area (K) in w^{1118} R24 discs and $Xrp1^{M2\text{-}73}$/+ R24 discs. w^{1118} n=10, $Xrp1^{M2\text{-}73}$/+ n=15. n.s. P>0.05. Scale bars are 100μm. Error bars are SEM. Statistical test used
778 was Welch's t-test.
779
780

S1

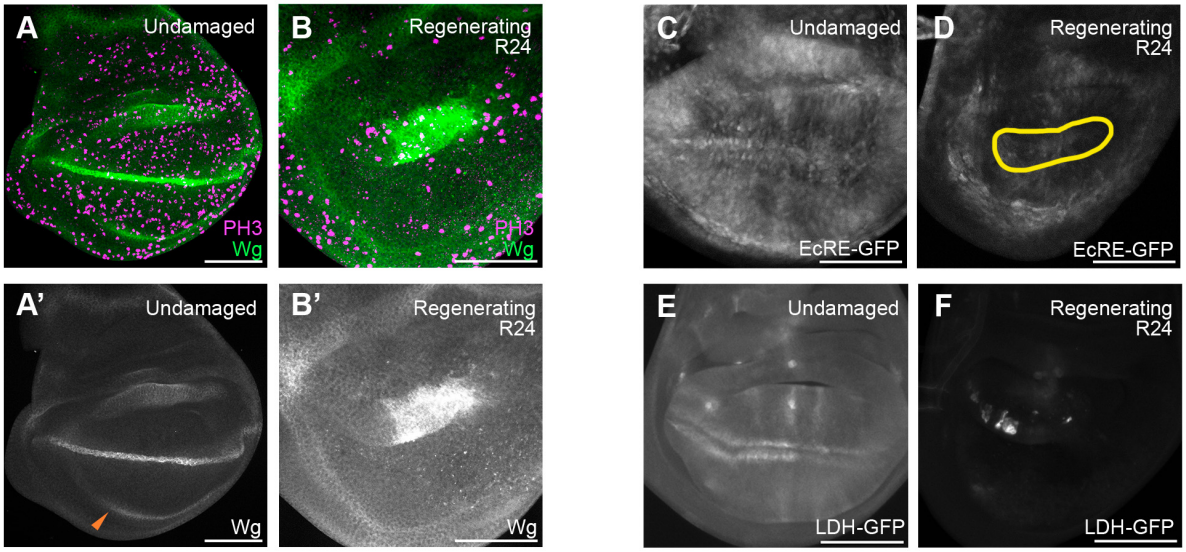

781 **Figure S1. Ecdysone receptor and Lactate dehydrogenase do not drive**
782 **regenerative growth**
783 (A-B') PH3 staining in an undamaged disc (A-A') and an R24 disc (B-B'). Orange
784 arrowhead in (A') indicates inner ring of Wg. (C-D) EcRE-GFP expression in an
785 undamaged disc (C) and an R24 disc (D). (E-F) LDH-GFP expression in an undamaged
786 disc (E) and an R24 disc (F).
787

S2

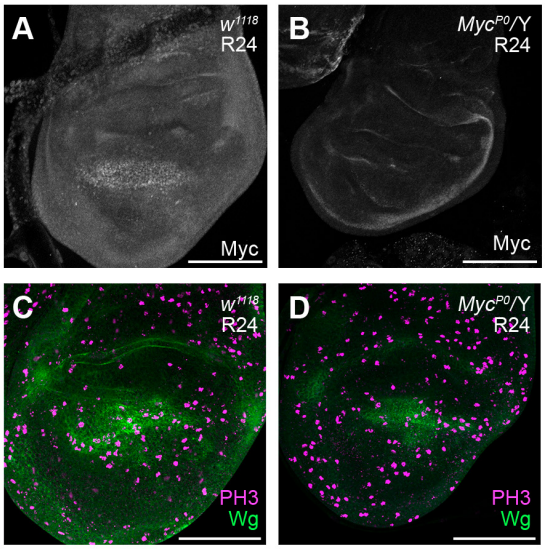

788 **Figure S2. The *Myc^{P0}* mutation reduces Myc and proliferation during regeneration**

789 (A-B) Myc immunostaining in a *w^{1118}* R24 disc (A) and a *Myc^{P0}/Y* R24 disc (B). (C-D)

790 PH3 staining in a *w^{1118}* R24 disc (C) and a *Myc^{P0}/Y* R24 disc (D).

791

S3

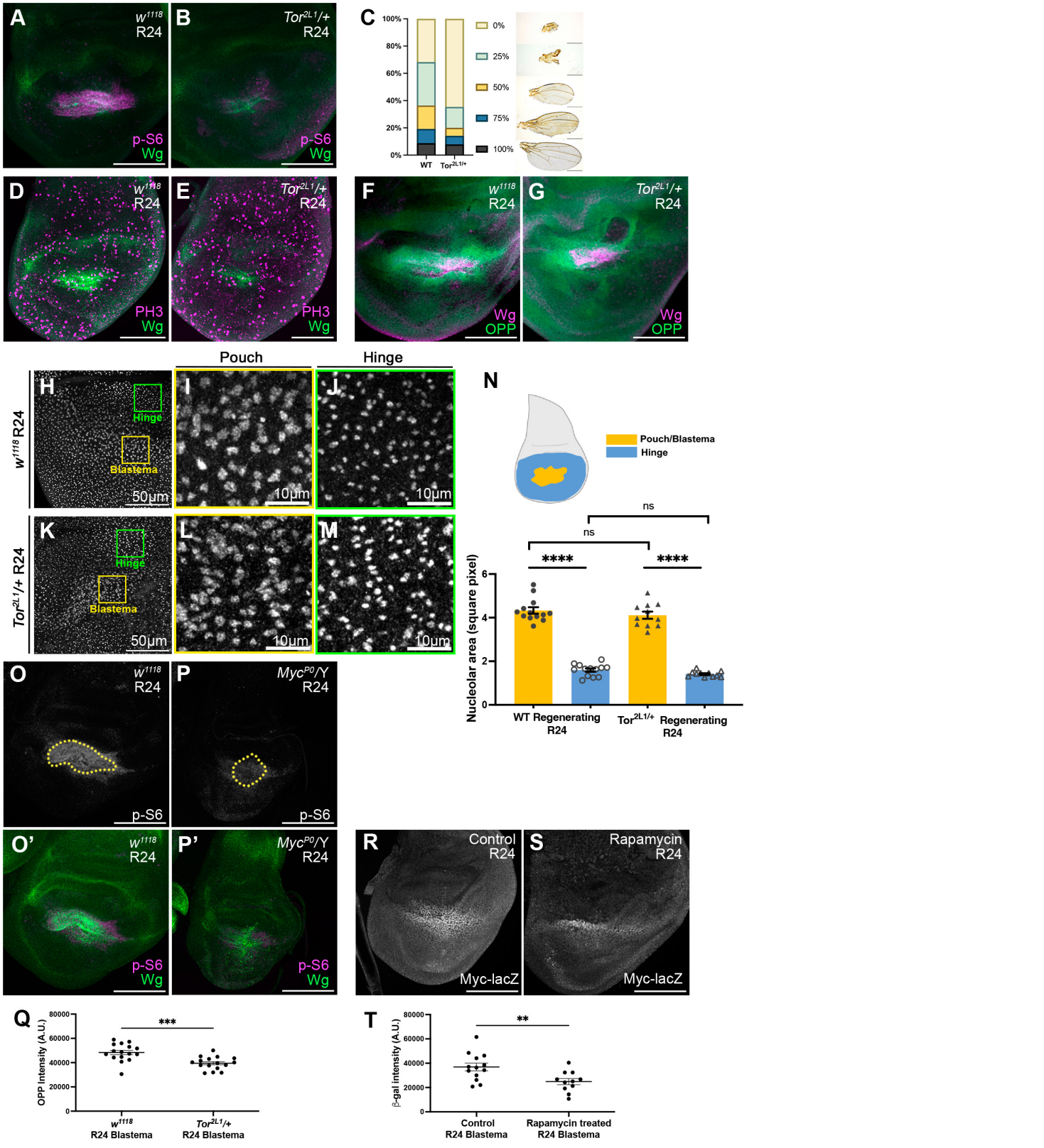

Figure S3. Effects of the *Tor^{2L1}* mutation on regeneration.

(A-B) p-S6 and Wg staining in a *w^{1118}* R24 disc (A) and a *Tor^{2L1}*/+ R24 disc (B). (C) Size of adult wings after disc regeneration in *w^{1118}* and *Tor^{2L1}*/+ animals. Scale bars are 500μm. (D-E) PH3 staining in a *w^{1118}* R24 disc (D) and a *Tor^{2L1}*/+ R24 disc (E). (F-G) OPP assay with Wg staining in a *w^{1118}* R24 disc (F) and a *Tor^{2L1}*/+ R24 disc (G). (H-M) Fibrillarin staining marking nucleoli in a *w^{1118}* R24 disc (H-J) and a *Tor^{2L1}*/+ R24 disc (K-M). (I, L) 200-pixel^2 area from blastema in H, K accordingly (yellow boxes), identified by Wg staining. (J, M) 200-pixel^2 area from wing hinge in H, K (green boxes). (N) Quantification of nucleolus size in hinge and blastema. Scale bars are 100μm unless otherwise marked. Error bars are SEM. (O-P) p-S6 staining in a *w^{1118}* (O) and a *Myc^{P0}/Y* (P) disc. (O'-P') p-S6 and Wg staining in a *w^{1118}* R24 disc (O') and a *Myc^{P0}/Y* R24 disc (P'). (Q) Quantification of average p-S6 staining intensity in the blastema identified by Wg staining (yellow dotted lines). n=10 *w^{1118}* n=10 , *Myc^{P0}/Y* n=9. **P<0.01. (R-S) *Myc-lacZ* expression marked by β-gal staining in a control R24 disc (R) and a rapamycin-treated R24 disc (S). (T) Quantification of average β-gal staining intensity in the blastema. control n=13, rapamycin n=11. **P<0.01. Statistical test used was Welch's t-test. Scale bars are 100μm unless otherwise marked. Error bars are SEM.

S4

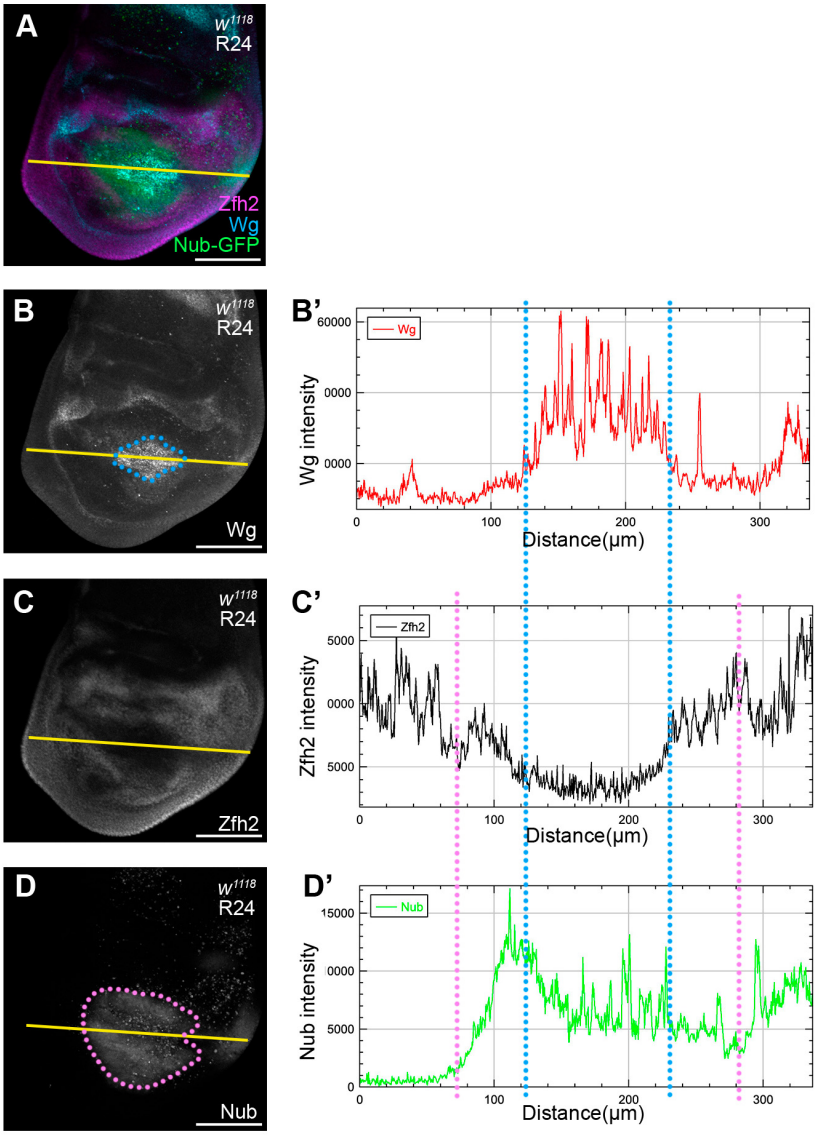

Figure S4. Map of Zfh2, Wg, and Nub expression.

(A) R24 disc expressing *nub-GFP* with Zfh2 and Wg immunostaining. (B) Wg staining. (B') Intensity plot of Wg staining taken from the yellow cross-section line in (B). (C) Zfh2 staining. (C') Intensity plot of Zfh2 staining taken from the yellow cross-section line in (C). (D) *nub-GFP* expression. (D') Intensity plot of GFP taken from the yellow cross-section line in (D). Blue dotted circle in (B) and blue dotted lines in (B'-D') indicate the edge of Wg-expressing area. Pink dotted circle in (D) and pink dotted lines in (C'-D') indicate edge of *nub-GFP* expressing area. Scale bars are 100μm.

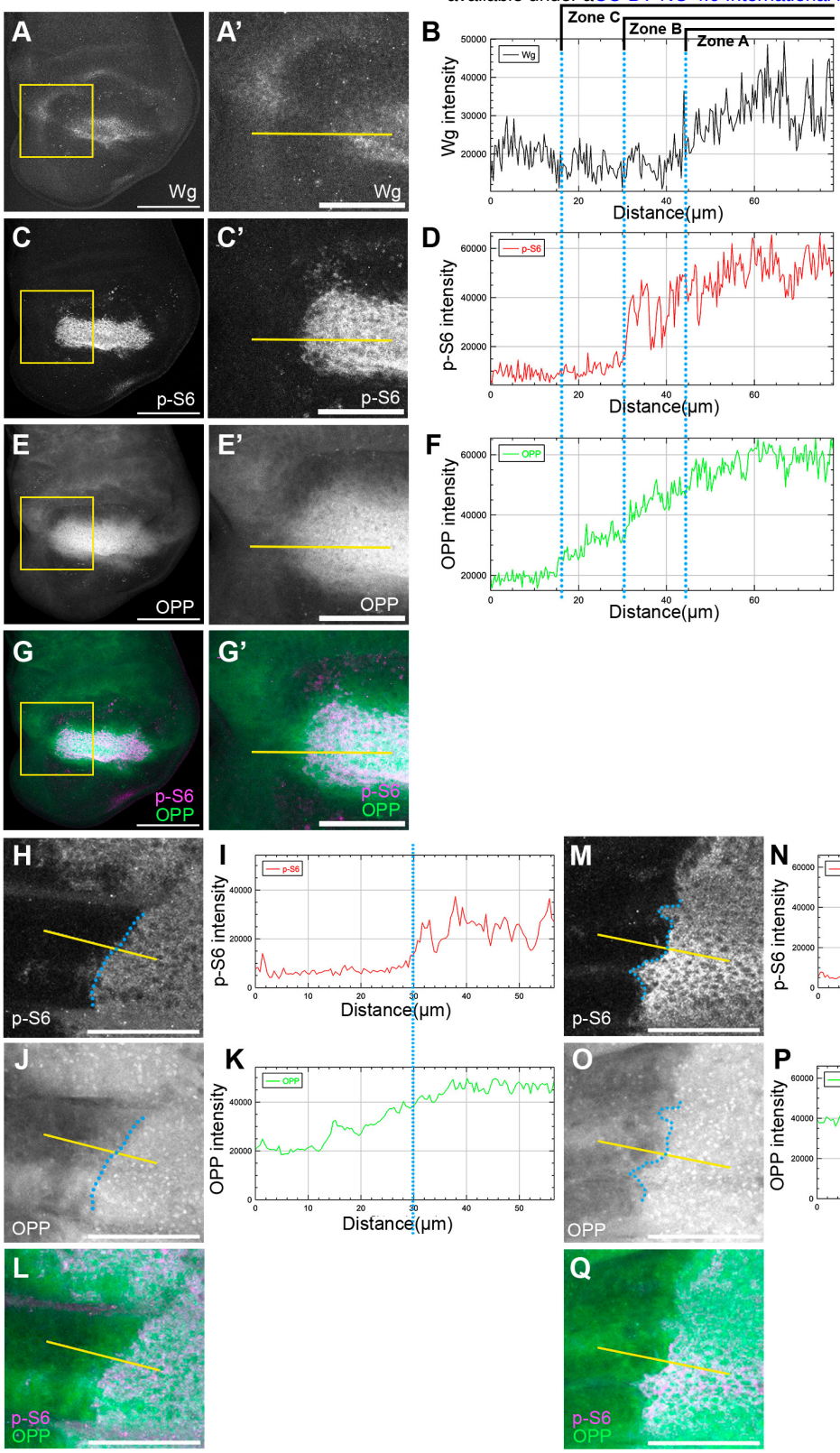

Figure S5. Map of Wg, p-S6, and OPP in the blastema.

(A,C,E,G) A *w*^{1118} R24 disc with Wg (A) and p-S6 (C) staining, OPP assay (E), and merge of p-S6 and OPP (G). (A',C',E',G') A higher magnification image of the yellow square in (A-G). (B,D,F) Fluorescence intensity plots taken from the yellow line in (A',C',E'). (H-Q) *hhGal4, UAS-Tsc2RNAi* (*hh>Tsc2i*) undamaged discs with p-S6 immunostaining (H, M) and OPP assay (J, O). Note (H-K) are from one wing disc and (M-Q) are from another wing disc. (I) Fluorescence intensity plot taken from the yellow line in (H). (K) Fluorescence intensity plot taken from the yellow line in (J). (N) Fluorescence intensity plot taken from the yellow line in (M). (O) Fluorescence intensity plot taken from the yellow line in (P). Blue dotted lines in (H-K) and (M-P) indicate the edge between high/low p-S6 staining. Scale bars are 100μm.

S6

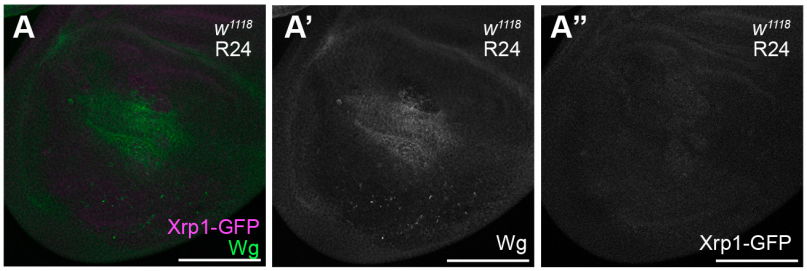

834 **Figure S6. Expression of Xrp1-GFP.**

835 (A-A") Xrp1-GFP expression in wing disc with Wg staining. (A) merge, (A') Wg, (A'')

836 GFP. Scale bars are 100μm.

837